

Methodology for Flow and Salinity Estimates in the Sacramento-San Joaquin Delta and Suisun Marsh

**37th Annual Progress Report
June 2016**

Chapter 4

Delta Salinity Simulation with DSM2-GTM

**Authors: En-Ching Hsu, Eli Ateljevich, and Prabhjot Sandhu
Delta Modeling Section
Bay-Delta Office
California Department of Water Resources**



Contents

4	Delta Salinity Simulation with DSM2-GTM.....	4-1
4.1	INTRODUCTION	4-1
4.2	EULERIAN ONE-DIMENSIONAL TRANSPORT SCHEME ALONG A CHANNEL REACH	4-1
4.2.1	Advection: Two-Step Lax-Wendroff Method.....	4-3
4.2.2	Reaction: Huen’s Method	4-5
4.2.3	Dispersion, Crank-Nicolson Method	4-5
4.2.4	Boundaries for the Full System.....	4-6
4.3	DELTA NETWORK ENHANCEMENTS FOR EULERIAN ONE-DIMENSIONAL TRANSPORT SCHEME	4-6
4.3.1	Delta Network Grid	4-6
4.3.2	Network Implications for Advection	4-7
4.3.3	Network Implications for Dispersion.....	4-8
4.3.4	Network Implications on Boundaries and Junctions.....	4-9
4.3.5	Reservoirs, Gates, and External Flows	4-11
4.4	LINKAGE TO DSM2-HYDRO AND OTHER DSM2-GTM CODE DESIGN CONSIDERATIONS	4-12
4.4.1	DSM2-HYDRO Tidefile.....	4-12
4.4.2	Time-Step Restrictions and Subcycling.....	4-12
4.4.3	Dispersion Coefficients.....	4-13
4.4.4	Multiple Constituents.....	4-14
4.5	DELTA SALINITY SIMULATION COMPARISON FOR DSM2-QUAL AND DSM2-GTM.....	4-14
4.5.1	Delta Historical Setup for Salinity Simulation	4-14
4.5.2	Results for Advection Only	4-16
4.5.3	Results Using DSM2-QUAL Calibrated Dispersion Coefficients.....	4-18
4.6	SENSITIVITY AND STABILITY TESTS	4-30
4.6.1	Sensitivity Analysis	4-30
4.6.2	Delta-scale Convergence Test.....	4-31
4.7	SUMMARY	4-33
4.8	ACKNOWLEDGEMENTS	4-34
4.9	REFERENCES	4-34

Tables

Table 4-1	Results for Convergence Test.....	4-17
-----------	-----------------------------------	------

Figures

Figure 4-1 Illustration of the Sequence for Operator Splitting.....	4-3
Figure 4-2 Illustration of Discretization for the Lax-Wendroff Method	4-3
Figure 4-3 DSM2-QUAL Grid in Contrast to DSM2-GTM Grid.....	4-7
Figure 4-4 Illustration of a Cell that is Located on a Multi-Channel Junction.....	4-8
Figure 4-5 Illustration of Tridiagonal Matrix in Contrast to Sparse Matrix.....	4-9
Figure 4-6 Electrical Conductivity Result Comparison at Martinez Outflow Boundary	4-10
Figure 4-7 Illustration of Reservoir in the Network System	4-11
Figure 4-8 Illustration of External Flows in the Network System.....	4-11
Figure 4-9 Delta Network for Historical EC Simulation.....	4-15
Figure 4-10 DSM2-GTM and DSM2-QUAL Simulated EC Results Comparison with Dispersion Off.....	4-17
Figure 4-11 EC Tidal Results Comparison among DSM2-GTM, DSM2-QUAL, and Observed Data at Emmaton and Jersey Point	4-19
Figure 4-12 EC Results Comparison among DSM2-GTM, DSM2-QUAL, and Observed Data at Middle River at Tracy.....	4-20
Figure 4-13 EC Results Comparison among DSM2-GTM, DSM2-QUAL, and Observed Data at Old River at Bacon Island.....	4-21
Figure 4-14 EC Results Comparison among DSM2-GTM, DSM2-QUAL, and Observed Data at Sacramento River at Collinsville	4-22
Figure 4-15 EC Results Comparison among DSM2-GTM, DSM2-QUAL, and Observed Data at Sacramento River at Emmaton.....	4-23
Figure 4-16 EC Results Comparison among DSM2-GTM, DSM2-QUAL, and Observed Data at Sacramento River at Rio Vista.....	4-24
Figure 4-17 EC Results Comparison among DSM2-GTM, DSM2-QUAL, and Observed Data at San Joaquin River at Antioch.....	4-25
Figure 4-18 EC Results Comparison among DSM2-GTM, DSM2-QUAL, and Observed Data at San Joaquin River at Jersey Point	4-26
Figure 4-19 EC Results Comparison among DSM2-GTM, DSM2-QUAL, and Observed Data at San Joaquin River at Stockton Ship Canal	4-27
Figure 4-20 Simulated Reservoir EC Comparison (Bethel, Clifton Court, and Discovery Bay).....	4-28
Figure 4-21 Simulated Reservoir EC Comparison (Franks Tract, Liberty, and Mildred).....	4-29
Figure 4-22 Sensitivity Analysis of Varying Sacramento Flow by 10 percent at Emmaton.....	4-30
Figure 4-23 Sensitivity Analysis of Varying SWP Pumping by 10 percent at Old River at Bacon Island	4-31
Figure 4-24 L_1 and L_2 Error Norms on Logarithmic Scale Plots	4-32

4 Delta Salinity Simulation with DSM2-GTM

4.1 Introduction

The California Department of Water Resources' Delta Modeling Section is developing a new DSM2 transport module, called the General Transport Model (DSM2-GTM). Progress on this effort was previously reported in Hsu et al. (2014). DSM2-GTM employs a fixed (Eulerian) mesh rather than one that moves with flow and follows virtual parcels of water in a Lagrangian scheme. The fixed grid will make it easier for this model to interact with other models, georeferenced data, data assimilation, optimization, and visualization as well as to couple inline to DSM2-HYDRO. It is also more straightforward to extend the new model to new physical processes with sediment, dissolved oxygen, and mercury cycling models that are currently being developed. Because of its extensibility, DSM2-GTM is expected to replace DSM2-QUAL.

Ateljevich et al. (2011) developed a prototype algorithm that includes a second-order two-step upwind method with a predictor-corrector operator-splitting approach. This is the algorithm employed for DSM2-GTM. Ateljevich et al. (2011) tested the algorithm with uniform, reversing, and synthetic tidal flows for single-channel problems of increasing complexity in terms of nonlinearity and spatial variation of parameters. They established that this algorithm integrates the transport equations with minimum numerical diffusion, and they also verified formal convergence properties of the scheme.

To extend the work to field-scale Delta problems and hydrodynamic data, changes were made to accommodate flow on a network of channels with varying cell size in different reaches to present an understandable interface and to improve the linkages with the DSM2-HYDRO model. To make the user transition from DSM2-QUAL to DSM2-GTM simpler, we intentionally imitated the input interface from DSM2-QUAL as closely as possible. The extra parameters, which have to be specified in DSM2-GTM, are requested cell size (dx) to generate the DSM2-GTM grid and time step (dt) to serve as the master time step for simulation. We modified the DSM2-HYDRO tidefile format used to transfer flow fields from DSM2-HYDRO to DSM2-GTM to improve its temporal and spatial resolution. (See Hsu et al. [2014] for details.) DSM2-QUAL dispersion coefficients are reusable in DSM2-GTM without change of scale; they depend on velocity and consequently have an interpretation that is slightly different from the classic constant dispersion factor (e.g., Fischer et al. 1979). This point is addressed in more detail in Liu and Ateljevich (2011). The translation between DSM2-QUAL and DSM2-GTM coefficients and classic dispersion coefficients is described in section 4.4.3.

Presently, DSM2-GTM produces results that are very consistent with DSM2-QUAL, which is an important initial milestone that allows us to release the model. We hope the adoption of the new model will be driven by a rapidly expanding toolset for analysis and by the emerging sediment and dissolved oxygen models.

4.2 Eulerian One-Dimensional Transport Scheme along a Channel Reach

In a collaborative project with University of California, Davis, Ateljevich et al. (2011) developed a second-order upwind one-dimensional Eulerian model of advection, dispersion, and reactions or sources. The advective-diffusive part of model describes basic conservative transport, and the generalized reaction term can be tailored to non-conservative water quality kinetics, including sediment transport.

The important mixing process in 1D channels is shear *dispersion* (see Fischer et al. 1979). On the other hand, in terms of the formulation, dispersion is usually represented by the so-called *diffusion analogy* so that when we talk about the partial differential equation, we use the terms *diffusion* and *advective-diffusion*. The term *numerical diffusion* refers to the spreading and dampening of the real solution

because the numerical method technically is a kind of error. But if it is modest compared with physical mixing, practitioners can absorb it into the dispersion parameters as part of calibration.

In conservative form, these are the equations.

$$\frac{\partial(A(x,t)C(x,t))}{\partial t} + \frac{\partial(Q(x,t)C(x,t))}{\partial x} = \frac{\partial}{\partial x} \left(A(x,t)K(x,t) \frac{\partial C(x,t)}{\partial x} \right) + A(x,t)S(x,t,C(x,t)) \quad (1)$$

↑
Time evolution

↑
Advection

↑
Dispersion

↑
Source/Reaction

where

x is distance along the channel,

t is time,

A is the cross-sectional area,

C is the scalar concentration,

Q is the flow,

K is the longitudinal dispersion coefficient modeled using the diffusion analogy,

S is the source or reaction term (deposition, erosion, lateral inflow, and other forms of sources and sinks) per unit area of a cross-section.

Eq. (1) describes the mass conservation of a pollutant in dissolved phase or suspended sediment away from the streambed. Boundary conditions will be discussed in sections 4.2.4 and 4.3.4.

A software testing framework was also developed for verifying the required accuracy of this solver over an incrementally more complex set of 1D flows, geometry, spatially varying-mixing parameters, and combinations of operators. The testing objective was to verify second-order accuracy, or be close to it, in both time and space on nonlinear problems, anticipating some degradation with more involved boundary conditions or over complex geometry.

An operator splitting-like approach was adopted for the solution, meaning that the advection, reaction, and dispersion processes are integrated sequentially in a specially orchestrated predictor-corrector sequence. The sequence is shown in Figure 4-1. The nature of the problem and the importance of the conservation of mass strongly suggested employing a Finite Volume Method (FVM). The algorithms employed for DSM2-GTM include a second-order two-step unwinding method with a van Leer slope limiter for advection, Heun's method for reaction, and then a final update including dispersion using a semi-implicit time discretization consistent with the Crank-Nicolson method. Although we use the term *operator splitting*, note that there is no succession of concentration updates, which is typical of fractional step methods like those used in DSM2-QUAL. Rather, we always considered all three sequences together, but we worked on advection first, reaction second, and finally on diffusion. This helped us avoid some of the pitfalls of traditional splitting methods, particularly at the boundary.

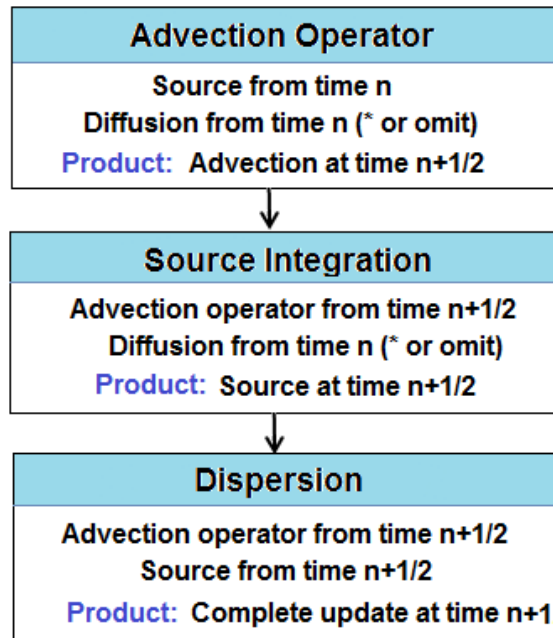


Figure 4-1 Illustration of the Sequence for Operator Splitting

4.2.1 Advection: Two-Step Lax-Wendroff Method

The Lax-Wendroff method is a numerical method for the solution of advection equations based on finite differences or volumes. It is second-order accurate in both space and time. The first predictor step calculates values at half-time step ($n+\frac{1}{2}$) and half-spatial step ($i \pm \frac{1}{2}$). This location represents the face between computational cells in the model. Two estimates are produced for each face, one from the perspective of the cell on each side. In the second step, the upwind flux is selected from each face, and the fluxes in and out of each cell are differentiated to form the flux divergence or the net change because of advection in and out. This dual-face concept is illustrated in Figure 4-2.

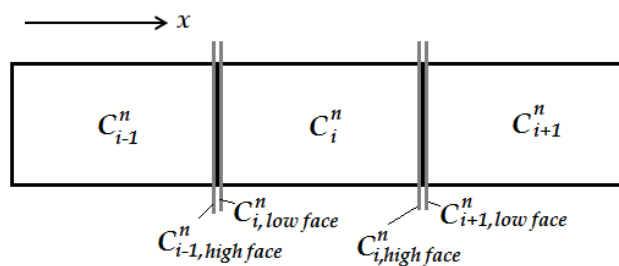


Figure 4-2 Illustration of Discretization for the Lax-Wendroff Method

The predictor step begins by estimating the concentration at the high- and low-side cell faces at the half-time step by using a Taylor expansion around the cell center.

$$C_{i\pm 1/2}^{n+1/2} = C_i^n \pm \frac{\partial C_i^n \Delta x}{\partial x \cdot 2} + \frac{\partial C_i^n \Delta t}{\partial t \cdot 2} \tag{2}$$

From Eq. (1), $\partial C/\partial t$ can be presented as

$$\frac{\partial C}{\partial t} = -\frac{Q}{A} \frac{\partial C}{\partial x} + \frac{1}{A} D^n + S^n \quad (3)$$

where

D^n denotes the explicit central difference discretization of the dispersion term in Eq. (1),

S^n is the source term evaluated at the old time step.

Substituting $\partial C/\partial t$, we can rewrite Eq. (2) as

$$C_{i\pm 1/2}^{n+1/2} = C_i^n + \frac{1}{2} \left(\pm 1 - \frac{\Delta t Q}{\Delta x_i A} \right) \Delta C_i^n + \frac{\Delta t}{2A} (D_i^n) + \frac{\Delta t}{2} S_i^n \quad (4)$$

The change of concentration ΔC_i^n is estimated based on the concentration from the adjacent cells $i-1$, i , and $i+1$ (Figure 4-2) with a second-order flux limiter $D(C_{limited})_i^n$ to avoid local overshoot from the second-order numerical scheme.

$$\Delta C_i^n = \frac{\partial C}{\partial x} \Delta x = D(C_{limited})_i^n \cdot \Delta x_i \quad (5)$$

We use generalizations of popular slope limiters applicable to our scheme and irregular spatial discretization, such as those studied by Berger et al. (2005). We used the total variation diminish (TVD) limiter in Berger et al. (2005), which gave a good balance between protection from oscillation and overshoot and dampening of the solution in our experiments. The gradients on the boundaries are approximated by one-sided differences with no limiting.

In our ultimate implementation, we currently dropped the explicit dispersion (D_i^n) from the predictor step. The presence of this operator rarely increased accuracy and seemed to be more sensitive to things like the mesh Peclet number, which is the ratio of advection to dispersion strength.

The prior step produces two estimates at each face, one from the cell above and one from the cell below. The “tie” is broken by choosing the estimate from the more-upwind cell according to the local velocity into the face. Once fluxes are determined at faces, the next step is to obtain a guess for the advection operator at time $(n+1)$ by using the extrapolated concentrations at half-time and half-space.

$$\left. \frac{\partial(QC)}{\partial x} \right|_i^{n+1/2} \cong \frac{QC_{i+1/2}^{n+1/2} - QC_{i-1/2}^{n+1/2}}{\Delta x_i} \quad (6)$$

The advection solver requires (or will accept) only a single boundary condition, and it will use the boundary condition only where there is inflow, which may change over time at a tidal boundary. The solver has been tested with Dirichlet (known concentration) boundary conditions. When the concentration at the boundary is known, it is swapped into Eq. (6), leading to a very straightforward calculation of the advective flux into the model.

4.2.2 Reaction: Huen's Method

The next term to be integrated is reaction. A reaction, or source term, could represent decay, interactions between constituents, or sediment suspension. It could also be used to model tributary flow, although we presently do not use it in this way.

Huen's method is used to integrate the source term. In this case, the source term is first calculated at the old time step, and a predictor update is carried out to advance the state variables (concentrations or mass) to the next time step.

$$\overline{AC}_i^{n+1} = AC_i^n - \Delta t \cdot \frac{QC_{i+\frac{1}{2}}^{n+\frac{1}{2}} - QC_{i-\frac{1}{2}}^{n+\frac{1}{2}}}{\Delta x} + \Delta t \cdot D_i^n + \Delta t \cdot AS_i^n \quad (7)$$

Note that in Eq. (7), we used our prior work on advection, but we still used the explicit representation of dispersion (alternatively, we dropped this term as described above). Once estimated concentrations are available at the new time step, a trial source at the new time (\bar{S}_i^{n+1}) can be computed and the final source ($S_i^{n+\frac{1}{2}}$) is an average of the old source and the new trial.

$$S_i^{n+\frac{1}{2}} = \frac{S_i^n + \bar{S}_i^{n+1}}{2} \quad (8)$$

4.2.3 Dispersion, Crank-Nicolson Method

The last step is the dispersion update. For this update, the advection and reaction updates from above are treated as fixed-source terms at the half-time (f).

$$f_i^{n+\frac{1}{2}} = -\frac{QC_{i+\frac{1}{2}}^{n+\frac{1}{2}} - QC_{i-\frac{1}{2}}^{n+\frac{1}{2}}}{\Delta x} + \frac{1}{2} \cdot [AS_i^n + A\bar{S}_i^{n+1}] \quad (9)$$

The remaining dispersion equation is calculated with the conventional Crank-Nicolson discretization in the FVM framework. It is unconditionally stable.

For this step, Eq.(1) is treated as follows,

$$\frac{\partial(AC)}{\partial t} = \frac{\partial}{\partial x} \left(AK \frac{\partial C}{\partial x} \right) + f \quad (10)$$

and discretized as follows in Eq. (11),

$$\begin{aligned} \frac{(AC)_i^{n+1} - (AC)_i^n}{\Delta t} &= \frac{\theta \Delta t}{\Delta x_i} \left\{ (AK)_{i+1/2}^{n+1} \left(\frac{C_{i+1}^{n+1} - C_i^{n+1}}{\Delta x_{i+1/2}} \right) - (AK)_{i-1/2}^{n+1} \left(\frac{C_i^{n+1} - C_{i-1}^{n+1}}{\Delta x_{i-1/2}} \right) \right\} + \\ &\frac{(1-\theta)\Delta t}{\Delta x_i} \left\{ (AK)_{i+1/2}^n \left(\frac{C_{i+1}^n - C_i^n}{\Delta x_{i+1/2}} \right) - (AK)_{i-1/2}^n \left(\frac{C_i^n - C_{i-1}^n}{\Delta x_{i-1/2}} \right) \right\} + f_i^{n+\frac{1}{2}} \quad (11) \end{aligned}$$

This can be rewritten in matrix form, which contains calculated coefficients, unknown variables, and calculated right-hand-side value, as shown in Eq. (12).

$$\begin{aligned} & \left[\frac{\theta \Delta t (AK)_{i-1/2}^{n+1}}{\Delta x_i \Delta x_{i-1/2}} A_i^{n+1} + \frac{\theta \Delta t}{\Delta x_i} \left[\frac{(AK)_{i+1/2}^{n+1}}{\Delta x_{i+1/2}} + \frac{(AK)_{i-1/2}^{n+1}}{\Delta x_{i-1/2}} \right] - \frac{\theta \Delta t (AK)_{i+1/2}^{n+1}}{\Delta x_i \Delta x_{i+1/2}} \right] \begin{bmatrix} C_{i-1}^{n+1} \\ C_i^{n+1} \\ C_{i+1}^{n+1} \end{bmatrix} \\ & = (AC)_i^n + f_i^{n+1/2} \cdot \Delta t - \frac{(1-\theta)\Delta t}{\Delta x_i} \left[F_{i+1/2}^n - F_{i-1/2}^n \right] \end{aligned} \quad (12)$$

where the diffusive fluxes (F) are given by Eq. (13),

$$F_{i+1/2}^n = -(AK)_{i+1/2}^n \left(\frac{C_{i+1}^n - C_i^n}{\Delta x_{i+1/2}} \right) \quad (13)$$

Dispersion requires a boundary condition at each boundary. The dispersion solver has been tested with both Dirichlet (known value) and Neumann (known flux or gradient) boundaries. For Dirichlet boundaries, the gradients are calculated over half of the cell (between its center and edge) rather than over a full cell (between the center and the neighbor's center). Neumann boundary conditions are implemented by preplacing the flux at the boundary face (say $F_{i+1/2}^n$) directly.

4.2.4 Boundaries for the Full System

Eq. (1) admits exactly one stipulated condition (Dirichlet or known value; Neumann or known flux) per boundary. This is not the same as the requirement for advection, which only allows a boundary at an inflow. There are potential consistency issues between the number and nature of boundary conditions that can be imposed. In particular, if one does what is convenient for the individual operators, the boundaries for the overall problem is likely to be overspecified, underspecified, or inaccurate (see, for instance, Leveque 2003). The symptoms we encountered at relatively active exit boundaries are convergence issues and numerical boundary layers, where concentration tends to pile up at the edge of the domain.

In all our tests, we used specified concentrations at inflow for both constructing the estimate of the advection operator and for diffusion. Then for outflows, we used no boundary for advection, and for diffusion we used a Dirichlet boundary, which is fixed by using extrapolated values from the interior. This treatment is technically underspecified, but seemed to allow second-order accuracy and some stability even with a fairly steep plume exiting the system. Boundaries for the Delta are covered in section 4.3.4.

4.3 Delta Network Enhancements for Eulerian One-Dimensional Transport Scheme

Prior work focused on a single channel with speculative software “hooks,” where the algorithm had to be patched together for use in a network. Additional work was needed to make the algorithm workable for production modeling in the Delta, including the provision of a flow field from DSM2-HYDRO, specification of the behavior at junctions, and connection to the DSM2 input system. The assumptions and enhancements are described below.

4.3.1 Delta Network Grid

To apply the scheme to the Delta network, features such as multiple boundaries, junctions, non-sequential cell numbering, gates, reservoirs, and external flows had to be considered.

The modification of Δx in different formulas is fairly straightforward. The irregularity comes into play when analyzing slopes across intermediate nodes (in the sense of Figure 4-3a), where the discretization is continued uninterrupted. Although we call it irregular, the spatial step is actually piecewise constant. It is the same along each channel with discontinuities between channels.

Along with the slopes, themselves, slope limiters also must be modified for spatially varying Δx . Slope limiters do exactly what they sound like they do: they limit the gradient of concentration that is assumed to exist in the cell and essentially exert a bound on calculations. They are used to guard against spurious oscillations and negative concentrations. Our original implementation was based on the van Leer limiter for uniform grids. There is no unique generalization to irregular grids; we used the limiter labeled “TVD” from Berger et al. (2005).

Because multi-channel junctions represent internal boundaries at cells adjoining multi-channel junctions (Figure 4-4), gradients are approximated by one-sided differences. For example, in cell i , the gradient is approximated solely from differences on the face shared with cell $i-1$. Multi-channel junctions are not rare, and we expected some trouble from this treatment, but it seems to produce acceptable results in practice. A well-studied alternate assumption is to assign the gradients around a multi-channel junction to be zero for the extrapolation step of the advection algorithm, which is the so-called Godonov first-order approximation. This simplification locally reduces the order of accuracy of advection across the junction. With a tidal system sloshing back and forth, error accumulates over time and becomes noticeable.

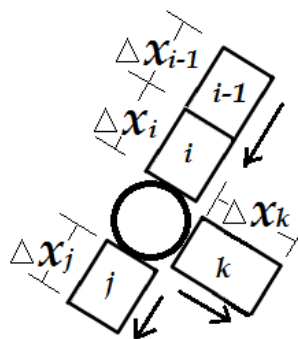


Figure 4-4 Illustration of a Cell that is Located on a Multi-Channel Junction

Notes: Δx_{i-1} , Δx_i , Δx_j , Δx_k = cell length of cell $i-1$, cell i , cell j , and cell k , respectively

To accommodate junction mixing, the average concentration of donor (upwind) flows moving into junctions is computed and assigned to the receiving cell faces. This is a mild expansion on the upwinding idea. Junction mixing is also used to apply external flows, which are channel depletions from consumptive-use.

Reservoirs are treated as fully mixed stirred tanks. This is the same approach that DSM2-QUAL has taken. The reservoir concentration is updated based on the assumption of instant mixing with all the connected donor flows.

4.3.3 Network Implications for Dispersion

Besides affecting the discretization length (Δx), the network potentially changes the nature of the linear algebra that has to be solved. For a single long channel, the dispersion discretization yields a matrix problem that is tridiagonal (Figure 4-5a). For certain treatments of the network problem where

dispersion is modeled across multi-channel junctions, the matrix is not tridiagonal but is merely sparse (Figure 4-5b), with the off-tridiagonal terms representing connections at nodes. To maintain sufficient flexibility to swap network formulations, we had to change solvers. We eventually decided to use the sparse matrix library KLU (Natarajan 2005), which is the same solver used for DSM2-HYDRO, to efficiently solve the sparse matrix. Little significant slowdown was observed by switching the solver and although our current treatment of dispersion can be recast as a series of tridiagonal problems, we prefer the flexibility of the sparse solver.

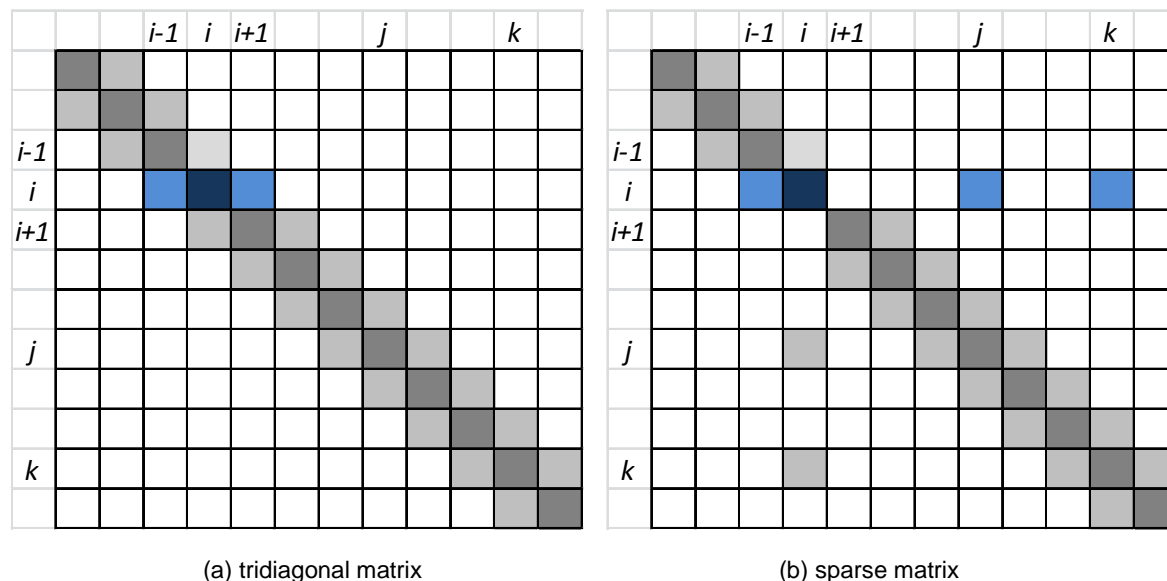


Figure 4-5 Illustration of Tridiagonal Matrix in Contrast to Sparse Matrix

Notes: $i-1$, i , $i+1$, j , and k = cell sequential numbers

4.3.4 Network Implications on Boundaries and Junctions

The external boundary and compatibility conditions over a 1D network require reasonable assumptions for implementation. . The following paragraphs describe our initial treatment for various categories of flow.

Inflow. Inflow boundaries are represented using Dirichlet boundaries (known values) for both the advection predictor step and for the final update including dispersion. The concentration, constant or time-varying, is given in the input system.

Outflow. The advection estimate requires no boundary condition. The full equation, along with dispersion, Eq. (1), requires a boundary condition. For the final update with dispersion, a Dirichlet boundary is used, but this is based on spatially extrapolated values rather than on input concentration. This treatment prevents the development of a numerical boundary layer because of the conflict between what is naturally emerging from the domain set off by strong advection and the stipulated boundary. Because no external value is imposed, the boundary is underspecified. Nonetheless, the method produces stable and accurate behavior in our tests, even as a significant plume exits the boundary. Our experiments suggest that alternate treatments only produce different results in a small

neighborhood of the boundary. The results using DSM2-GTM is an improvement over DSM2-QUAL near the tidal boundary during outflow (Figure 4-6). DSM2-QUAL assumes zero dispersion at the boundary.

Intermediate nodes. In many ways, it is fair to say intermediate junctions are not treated as boundaries in DSM2-GTM. Tributary mass sources, such as consumptive-use, are added as part of the junction mixing described above, and a discontinuity occurs in the discretization length (dx). In DSM2-QUAL, no mixing occurs across either intermediate nodes or junctions; at the same time, the junction treatment in DSM2-QUAL provided numerical diffusion, apparently achieving the same end.

Multi-channel (true) junctions. For advection, a multi-channel (true) junction is treated as a coupled inflow and outflow boundary for advection with appropriate mixing, which was elaborated in the previous section. A homogenous Neumann boundary condition (zero diffusive flux) is imposed on dispersion. The zero dispersion assumption is the same one used in DSM2-QUAL at all nodes. The assumption circumvents numerous practical issues defining exactly how dispersion should be defined and how mass should be conserved from both advection and dispersion. The treatment produces acceptable results more than other treatments we tested compared with field data, but it clearly interrupts a physical process and may be a possible area of improvement in the future.

For a Delta simulation, the inflow boundaries are Yolo Bypass and the Sacramento (Freeport), San Joaquin (Vernalis), Calaveras, Mokelumne, and Cosumnes rivers. Martinez is a tidal boundary and is periodically an inflow or outflow. Exports and diversions include the State Water Project (SWP) Banks Pumping Plant, Central Valley Project (CVP) Tracy Pumping Plant, North Bay Aqueduct exports, and Contra Costa Water District diversions. They are treated as outflow boundaries or external flows with junction water mixing depending on whether they lie at the end of a channel.

DSM2-GTM reported the salinity at the Martinez outflow location matched the input boundary data well, while DSM2-QUAL reported artificial drops in salinity because of the limitation of parcel formation. This can be seen in Figure 4-6.

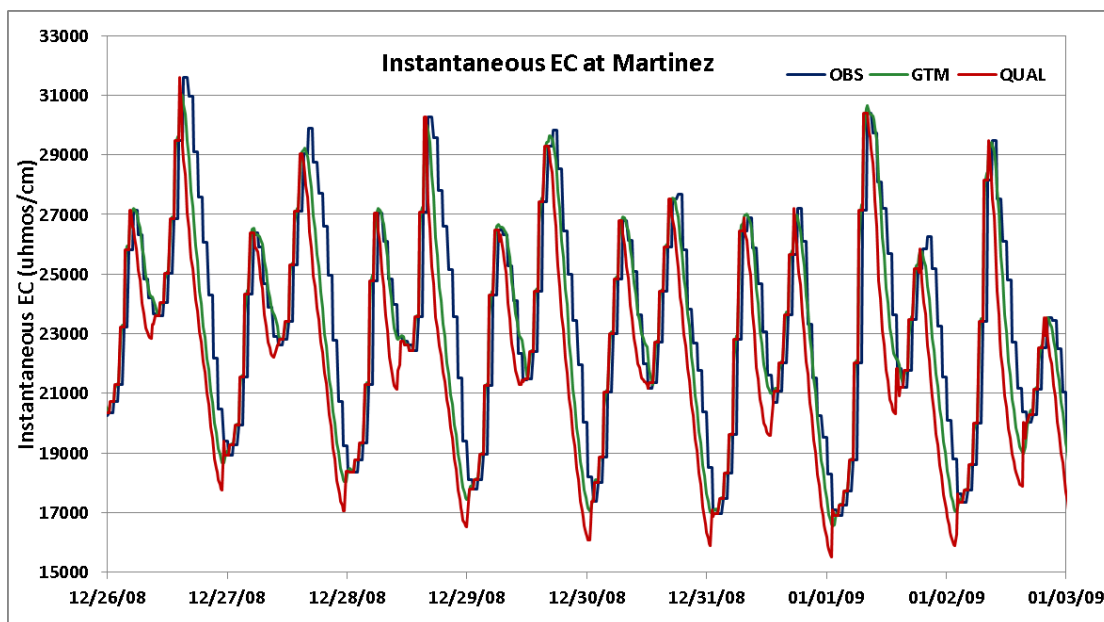


Figure 4-6 Electrical Conductivity Result Comparison at Martinez Outflow Boundary

Notes: OBS = data observed, GTM = DSM2-GTM, QUAL = DSM2-QUAL, EC = electrical conductivity, umhos/cm = micromhos per centimeter

4.3.5 Reservoirs, Gates, and External Flows

Reservoirs are treated as fully mixed volumes. Figure 4-7 is an example of how the connected flows to a reservoir in DSM2 are specified. The calculation is a simple mass-balance equation around a reservoir, as shown in Eq. (14).

$$C_R^{n+1} = \frac{V_R^n \cdot C_R^n + \sum_i Q C_i^{n+\frac{1}{2}} \cdot \Delta t}{V_R^{n+1}} \tag{14}$$

where

V_R^n is the reservoir volume at time (n),

C_R^n is the reservoir concentration at time (n),

the connected flows (Q) include external flows directly dumping into the reservoirs and flows from connected channels.

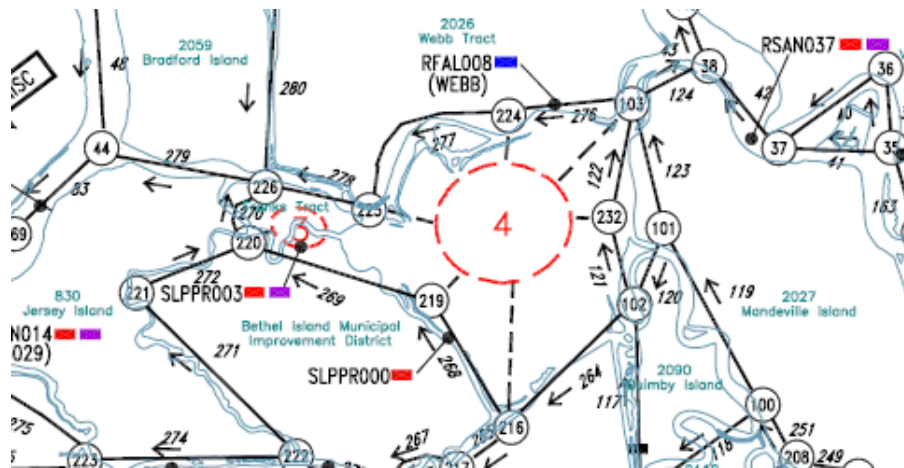


Figure 4-7 Illustration of Reservoir in the Network System

External flows, such as channel depletions from DICU (Delta Island Consumptive-Use), are added to junction mixing, as described previously. The mixed concentration to be assigned to the low face of cell j is calculated based on the external flows and concentrations entering from the high face of cell i (Figure 4-8). Note that agricultural flows are not implemented using the source term.

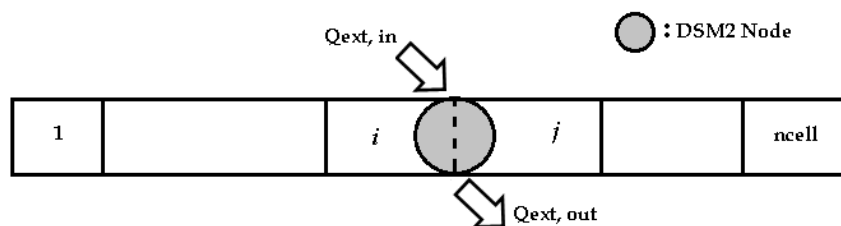


Figure 4-8 Illustration of External Flows in the Network System

Notes: 1, i , j , ncell = cell No., $Q_{ext, in}$ = external flow added to the junction, $Q_{ext, out}$ = external flow left the junction

Gates are not treated specially in DSM2-GTM for advection beyond their role in DSM2-HYDRO for determining flow. The dispersion coefficient around the gate is re-assigned to zero to avoid artificial diffusive fluxes across gates.

4.4 Linkage to DSM2-HYDRO and other DSM2-GTM Code Design Considerations

DSM2-GTM is written in Fortran 90 and is intended to be a flexible and reusable model, which enables a relatively easy integration of additional water quality parameters. Constituents can be added by writing a handful of subroutines governing the initialization, reaction, and output of those constituents.

To ease the transition from DSM2-QUAL to DSM2-GTM from a user's perspective, DSM2-GTM adopts an input and output system that is similar to the existing input/output (I/O) in DSM2-QUAL. The input system is based on a text reader using keywords that will seem familiar to users of DSM2-QUAL. Current DSM2-QUAL users can apply their existing studies with minimal changes in the input file.

4.4.1 DSM2-HYDRO Tidefile

This project was considered a good opportunity to update hydrodynamic information included in the DSM2-HYDRO output tidefile, which is the DSM2 name for the file that transmits results from DSM2-HYDRO to DSM2-QUAL. DSM2-HYDRO has already been modified to provide a lossless hydrodynamic representation in the DSM2-HYDRO tidefile (Hsu et al. 2014). Additional changes that have been made are:

- Hydrodynamic spatial representations are output on every DSM2-HYDRO computational point instead of coarser DSM2 map nodes.
- Hydrodynamic representations are instantaneous values rather than theta average quantities.
- Area has been eliminated as a state variable because it was redundant. We now include only water surface, plus sufficient geometry information, to reproduce the calculation of the cross-sectional area in DSM2-HYDRO.

The spatial resolution of DSM2-GTM is much more precise than that of DSM2-HYDRO. Even with a lossless transfer, the flow field provided by DSM2-HYDRO is incompletely specified and requires interpolation. Our approach starts by interpolating water-surface elevation. The area is then calculated based on geometry and water surface. Once area is determined for all grids, flow is obtained by linear interpolation between two DSM2-HYDRO computational points. The interpolation is not conservative, although deviations are minimal. We expect to eventually move to a conservative projection-based model.

4.4.2 Time-Step Restrictions and Subcycling

In transport problems, the Courant-Friedrichs-Lewy (CFL) condition describes the time step required for stability while solving for advection. For a one-dimensional problem, the CFL condition has the following form.

$$CFL = \frac{u\Delta t}{\Delta x} \leq C_{max} \quad (15)$$

where

u is the magnitude of the velocity,

Δt is the time step,

Δx is the space interval,

C_{max} depends on the method used to solve the discretized equation, such as whether the method is explicit or implicit. Typically, $C_{max}=1$ for an explicit solver, which for the spatial discretization reported here amounts to a fairly mild restriction.

In intuitive terms, the CFL condition for our algorithm says that fluid may not be transported by the mean velocity more than one DSM2-GTM computational cell in one time step. Since the possibility of this happening somewhere over a large channel network is common and difficult to anticipate, most practical models that use explicit time stepping include some form of subcycling, meaning that the model automatically discovers and uses the largest stable step that effectively divides the overall global time step.

4.4.3 Dispersion Coefficients

The parameterization of dispersion in DSM2-GTM comes from DSM2-QUAL and its predecessor, Branched Lagrangian Transport Model (BLTM). DSM2 Version 8.1 consolidated the mixing formulation for DSM2-QUAL (Liu and Ateljevich 2011) to achieve consistency with an underlying partial differential equation. Advection has been dropped for this discussion. The component used to calculate the parcel exchange diffusive flux is

$$\frac{\partial C}{\partial t} = \frac{1}{A} \frac{\partial}{\partial x} \left(DC \cdot |Q| \cdot \frac{\partial C}{\partial x} \right) \quad (16)$$

where DC is a parameter described below. The general accepted form of 1-D river dispersion can be written as

$$\frac{\partial C}{\partial t} = \frac{1}{A} \frac{\partial}{\partial x} \left(A \cdot K \cdot \frac{\partial C}{\partial x} \right) \quad (17)$$

where

C is the concentration,

t is the time coordinate,

K is the classic longitudinal dispersion coefficient.

Comparing Eq. (16) and Eq. (17), we get the following two relationships.

$$DC \cdot |Q| = A \cdot K \quad (18)$$

or

$$K = DC |\bar{u}| \quad (19)$$

where \bar{u} is the mean cross-sectional velocity.

The coefficient DC is the one traditionally used as the input dispersion coefficient in DSM2 Version 8.1. In DSM2-GTM, it is converted to K by multiplying by velocity magnitude. In most of the Delta, where tidal dispersion and junction mixing prevail as the key mixing factors, the modulation of dispersion by velocity seems reasonable. One advantage to the described approach is that the dispersion coefficient, Eq. (20), is proportional to velocity, which means the mesh Peclet number (Pe),

$$Pe = \frac{|u| \cdot \Delta x}{K} = DC \Delta x, \quad (20)$$

stays constant over time. The Peclet number measures the ratio of transport because of advection and dispersion. The performance of the algorithm is more consistent when it varies less, which is a point that was also noted as an advantage for QUAL/BLTM (Jobson and Schoellhamer [1987]). The code has been arranged so that it would not be difficult to replace this parameterization with another code, perhaps to recognize the link between longitudinal salinity profiles and mixing.

4.4.4 Multiple Constituents

This transport model has been designed to allow multiple constituents. DSM2-GTM relegates the reactions between constituents to external modules. The modules in development include a sediment, dissolved oxygen, temperature, and mercury cycling module.

4.5 Delta Salinity Simulation Comparison for DSM2-QUAL and DSM2-GTM

In a previous report (Hsu et al. 2014), a number of simple test cases were designed to evaluate the behavior of DSM2-GTM over simple networks, and the results were compared with DSM2-QUAL. Since then, the effort has been on field testing with salinity.

4.5.1 Delta Historical Setup for Salinity Simulation

The historical setup used in this study was obtained from DSM2 Version 8.1, which incorporates the latest improvements to the DSM2 code and a new calibration with NAVD88 datum (Liu et al. 2013). The conversion to NAVD88-stage datum improved the comparison of predicted and observed stages in the Delta. Errors in Clifton Court Gate operation data, Martinez stage data, and Martinez electrical conductivity (EC) data were corrected. Liu concluded that DSM2-QUAL Version 8.1 predicted EC at key stations in the Central Delta (Collinsville, Emmaton, Antioch, and Jersey Point) fairly well. The new results using calibrated DSM2-GTM are generally very close to the historical calibration results.

The simulation period for the tests is January 1, 1999–April 1, 2012. The map of the Delta network and the key locations we used for comparison are shown in Figure 4-9. The setup includes all boundary flows with Martinez boundary stage, SWP and CVP pumping, DICU flows, reservoirs, and gates.



name	Location	Name	Location
RMID027	Middle River at Tracy Rd	RSAC101	Sacramento River at Rio Vista
ROLD024	Old River at Bacon Island	RSAN007	San Joaquin River at Antioch
RSAC081	Sacramento River at Collinsville	RSAN018	San Joaquin River at Jersey Point
RSAC092	Sacramento River at Emmaton	RSAN058	Stockton Ship Canal

Figure 4-9 Delta Network for Historical EC Simulation

4.5.2 Results for Advection Only

To evaluate the diffusive influence of the algorithms and junction mixing, it was of interest to investigate how DSM2-GTM compares with DSM2-QUAL with dispersion turned off, so that salt is transported by advection only. For this test, the upstream concentrations and agricultural sources are set to zero, so that numerical diffusion can be investigated qualitatively.

The results are shown in Figure 4-10 after the model has been integrated for 13 years of simulation. Though the results are associated with field stations, the values at these stations are not representative of field conditions. Ocean forcing could bring a fairly significant salinity amount within a tidal excursion of Martinez, which would be enough to reach Pittsburg or Antioch, but there is generally average flow out of the domain. One criterion of success for this test was extra numerical diffusion from advection would not bring an objectionable flux of salt landward to those points where it might be expected to have a physical effect. The results of DSM2-GTM and DSM2-QUAL are very similar for this test. Both models still show salinity of 300 micro Siemens per centimeter ($\mu\text{S}/\text{cm}$) at Emmaton and some salinity amounts peak around 10 micromhos per centimeter ($\mu\text{mho}/\text{cm}$) at Rio Vista. During high flow season, both model results indicate that water becomes fresh and salt leaves the system. For the low flow season in the inner Delta, the numerical diffusion leads to conductivity of no more than a few $\mu\text{S}/\text{cm}$. Overall, this test, with consumptive-use turned off, suggests numerical diffusion is well controlled, presenting a less-than-first-order effect compared to advection. Other tests with consumptive-use enabled suggest that plume advection around the Delta is also very consistent between models.

The results of this test were encouraging for both models. DSM2-QUAL uses a Lagrangian scheme, which moves salt by simply tracking parcels as they move with the flow. Since the parcels don't spill into one another when the model is operated with mixing turned off, it is often touted as being a perfect numerical scheme with zero numerical diffusion. Be that as it may, the authors were concerned how this label of perfection would hold up in the context of time-varying flow and intermediate junctions. This is because DSM2-QUAL accuracy is limited by the quality of hydrodynamic information, the ability to track the parcels relative to locations of interest, and by certain *ad hoc* features of the model, such as recombination of small parcels. All of these limitations are associated with the treatment of flow as it passes Eulerian landmarks, such as map nodes. In contrast, DSM2-GTM is less affected by extra map nodes, but it is susceptible to numerical diffusion. The consistency between the two schemes in the Western Delta and the low intrusion into the Central Delta during this test confirms that numerical diffusion is sufficiently low in both models, such that numerical diffusion from the advection step is not muddled with dispersive mixing. To the extent that there is numerical diffusion, it likely comes from the common feature of the two models, which mixes fluxes as they flow across multi-channel junctions joining tributaries, as shown in Figure 4-3.

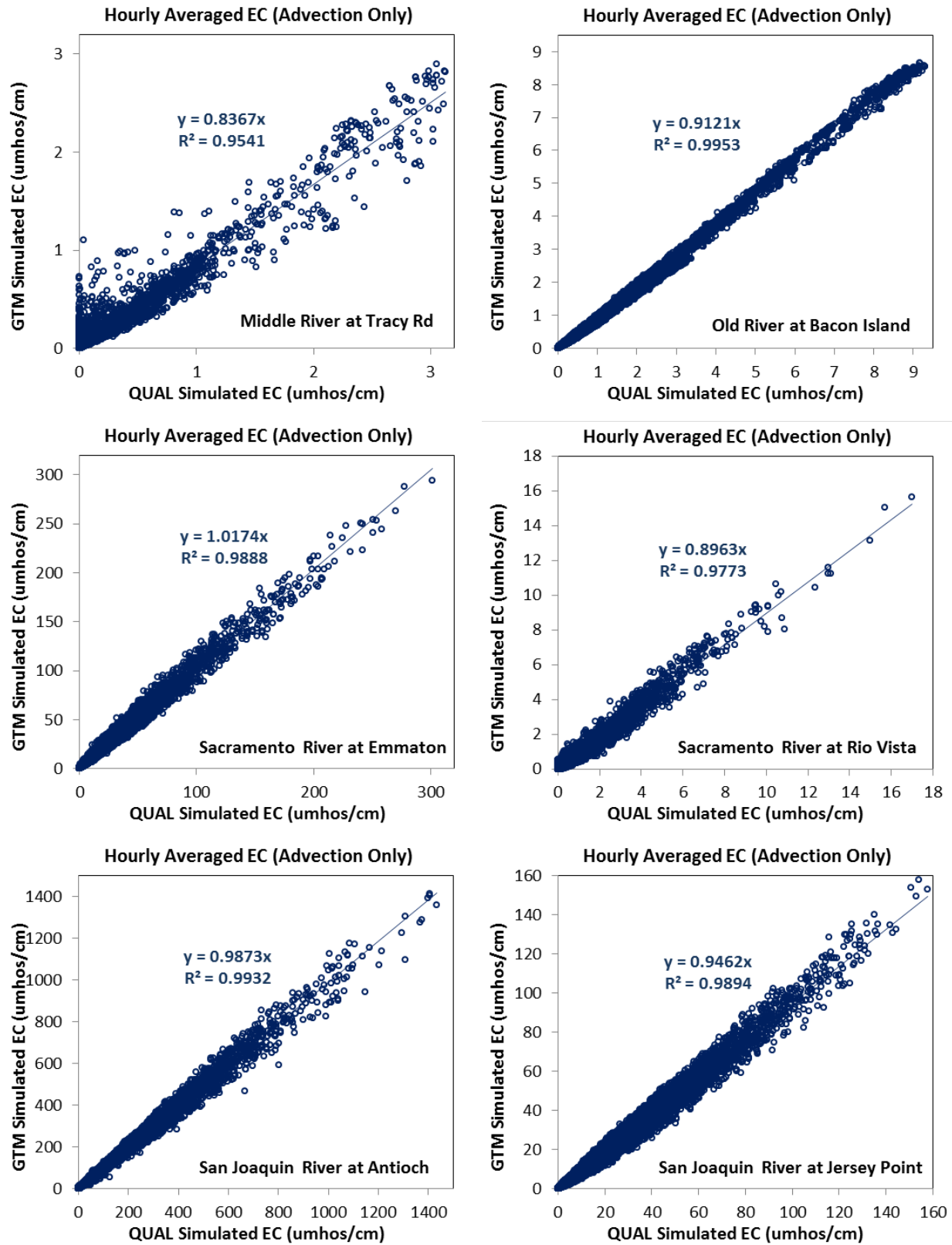


Figure 4-10 DSM2-GTM and DSM2-QUAL Simulated EC Results Comparison with Dispersion Off

4.5.3 Results Using DSM2-QUAL Calibrated Dispersion Coefficients

At this stage of development, DSM2-GTM has not been independently calibrated. The dispersion coefficients used for testing and comparison in this chapter are from the historical calibration for DSM2 Version 8.1 (Liu et al. 2013) that were used in DSM2-QUAL. The calibration period was October 1, 2000—October 1, 2008. All the available stations with good data were used so that the calibration covers most locations of interest.

The detailed tidal dynamics can be observed from those 15-minute instantaneous values. The tidal results at Emmaton and Jersey Point are shown in Figure 4-11. The plots indicate that DSM2-GTM and DSM2-QUAL both capture the low/high high tides and low/high low tides fairly well, with respect to the trend and the amplitude.

Figure 4-9 shows the locations in the Delta network by DSM2 output labels for the simulations. Simulation results for Middle River at Tracy Road (RMID027), Old River at Bacon Island (ROLD024), Sacramento River at Collinsville (RSAC081), Emmaton (RSAC092), Rio Vista (RSAC101), San Joaquin River at Antioch (RSAN007), Jersey Point (RSAN018), and Stockton Ship Canal (RSAN058) are shown in Figures 4-12 through 4-19. There are three subplots in each figure. The top right monthly averaged EC time-series plot compares DSM2-GTM results with DSM2-QUAL and observed data (OBS). The top left plot is the scatter plot of monthly averaged EC. The bottom plot is a time-series plot for daily averaged EC. Overall, the simulation results from DSM2-GTM overlap the results from DSM2-QUAL. There have been decades of studies on DSM2-QUAL, which produced improvements and calibrations in DSM2-QUAL, and its ability to match historical data is well understood. DSM2-GTM producing results, which are close to DSM2-QUAL results, is an important milestone.

We also studied reservoir concentration. The computational approach for DSM2-QUAL and DSM2-GTM is the same. As long as the EC results of the connected channels are similar, the reservoir concentration are not expected to differ much. The concentrations for Bethel, Clifton Court, Discovery Bay, Franks Tract, Liberty, and Mildred are shown in Figures 4-20 and 4-21. The results from DSM2-GTM and DSM2-QUAL are fairly close as expected. There is an obvious discrepancy observed for Discovery Bay and that was expected because there are differences between DSM2-QUAL and DSM2-GTM for the channels in that region. This is where DSM2-GTM calibration is needed.

Because the parameters from the previous DSM2-QUAL calibrations are initial estimates, this makes calibrating DSM2-GTM easier. There are some problems in South Delta regions to match observed data. These are also problematic areas for DSM2-QUAL to match EC results as well because many of the issues have to do with hydrodynamics and consumptive-use and not the transport scheme or dispersion coefficient.

Judging from Figures 4-12—4-19, it is clear DSM2-GTM often has slightly higher EC values than DSM2-QUAL. There was an attempt to scale this down by multiplying the dispersion coefficient by 0.9. Doing that shifts the EC down a bit for most key locations, but we decided to leave this type of test to full calibration.

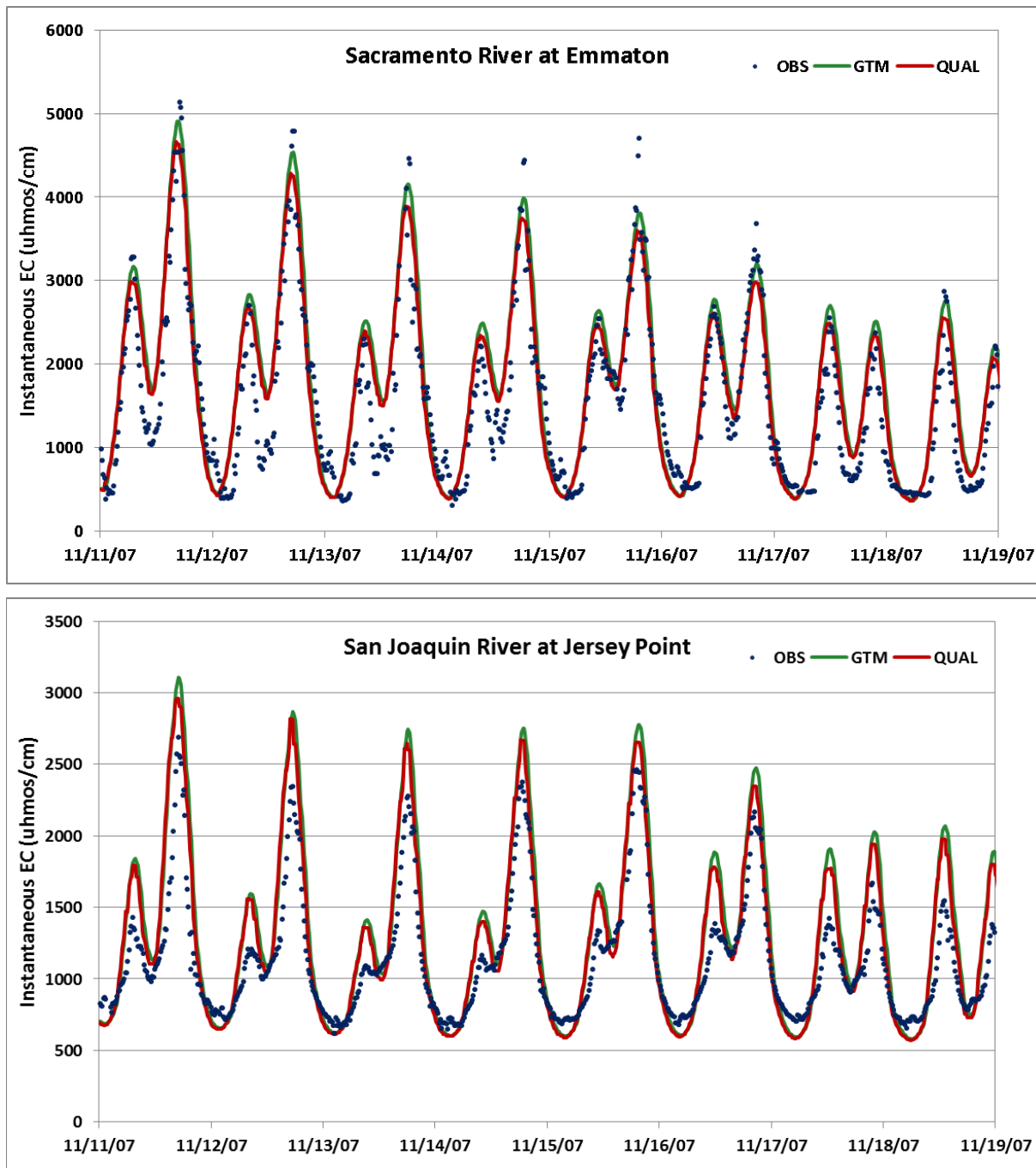


Figure 4-11 EC Tidal Results Comparison among DSM2-GTM, DSM2-QUAL, and Observed Data at Emmaton and Jersey Point

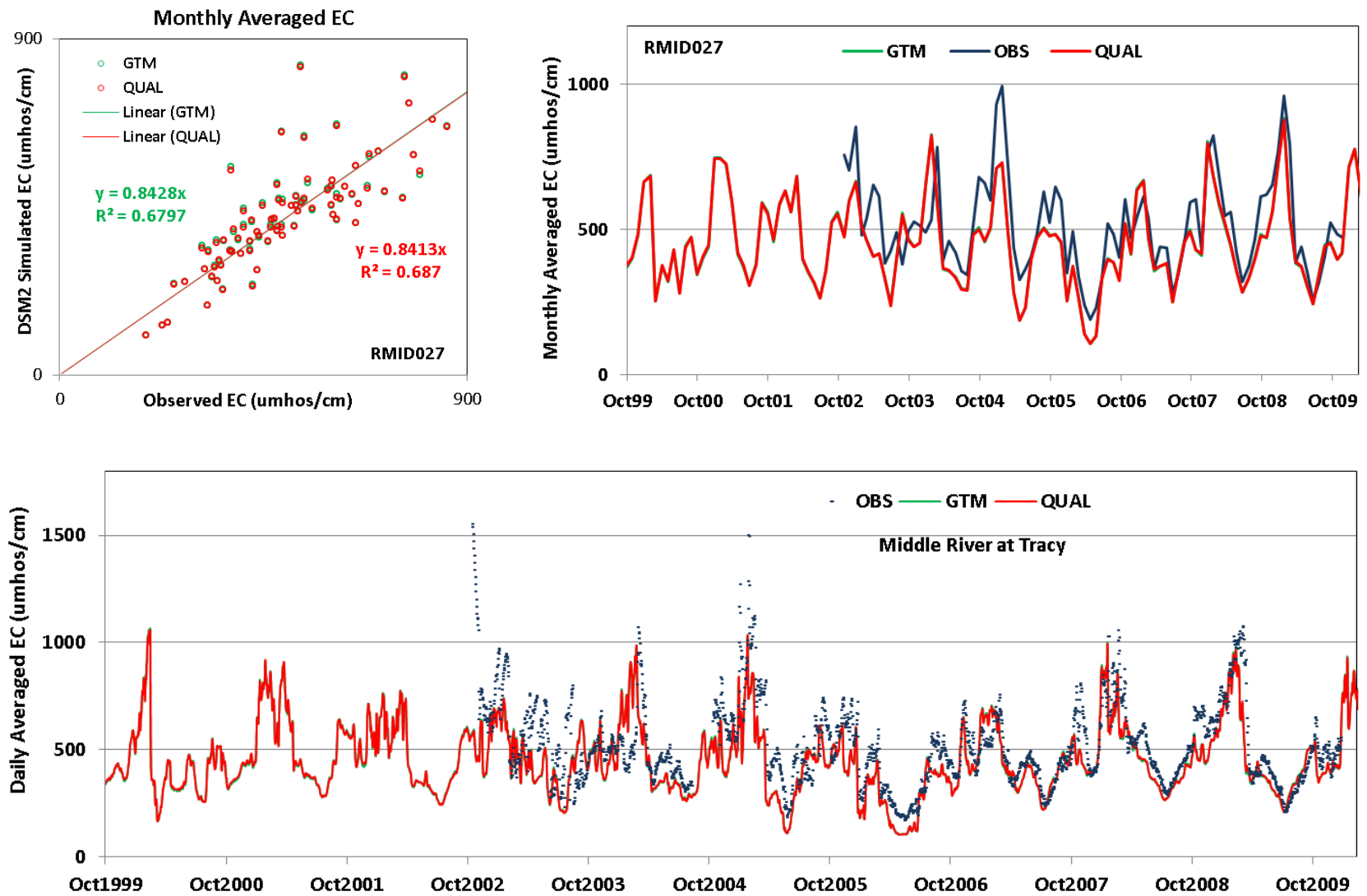


Figure 4-12 EC Results Comparison among DSM2-GTM, DSM2-QVAL, and Observed Data at Middle River at Tracy

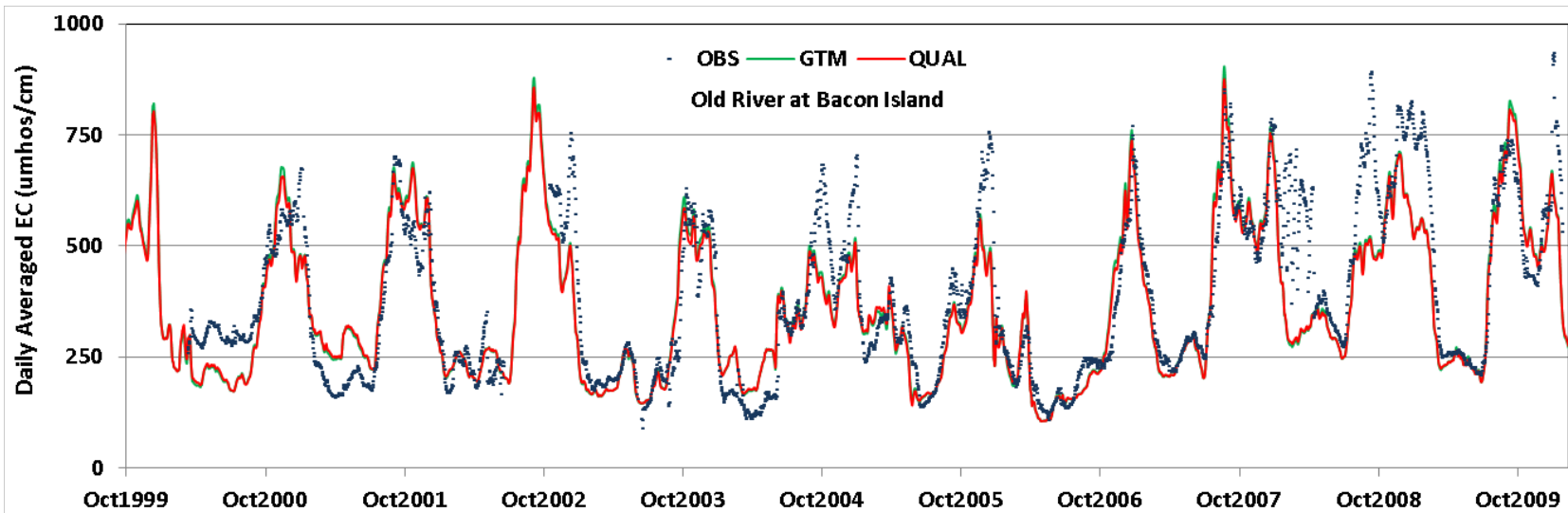
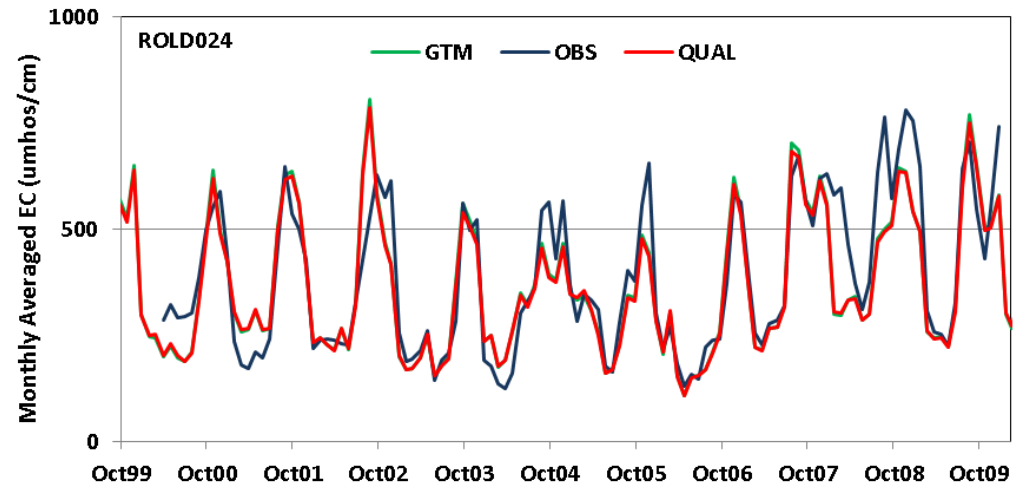
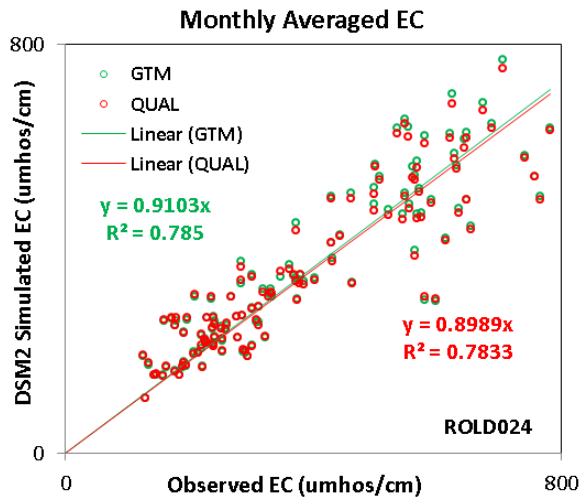


Figure 4-13 EC Results Comparison among DSM2-GTM, DSM2-QUAL, and Observed Data at Old River at Bacon Island

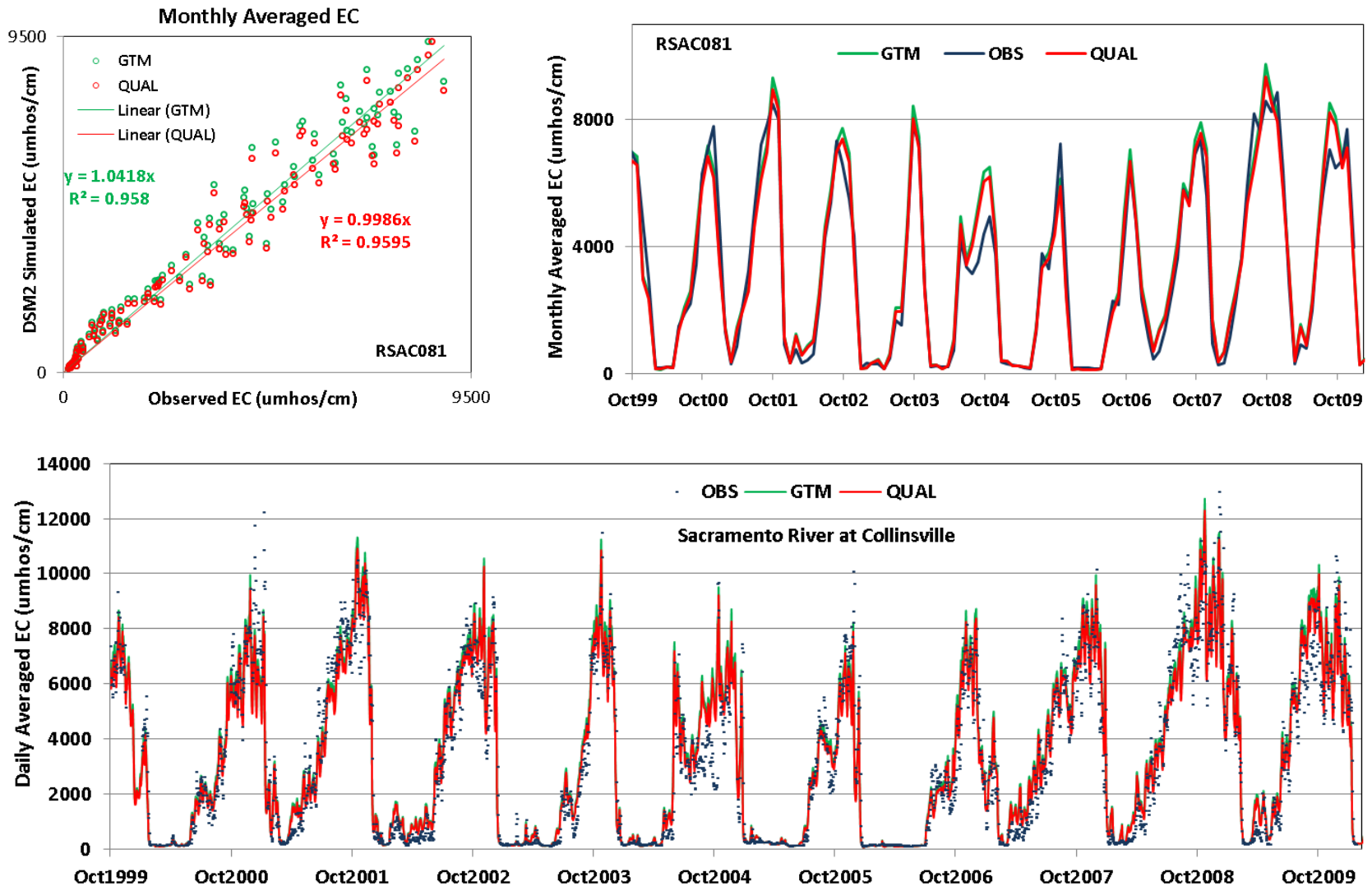


Figure 4-14 EC Results Comparison among DSM2-GTM, DSM2-QUAL, and Observed Data at Sacramento River at Collinsville

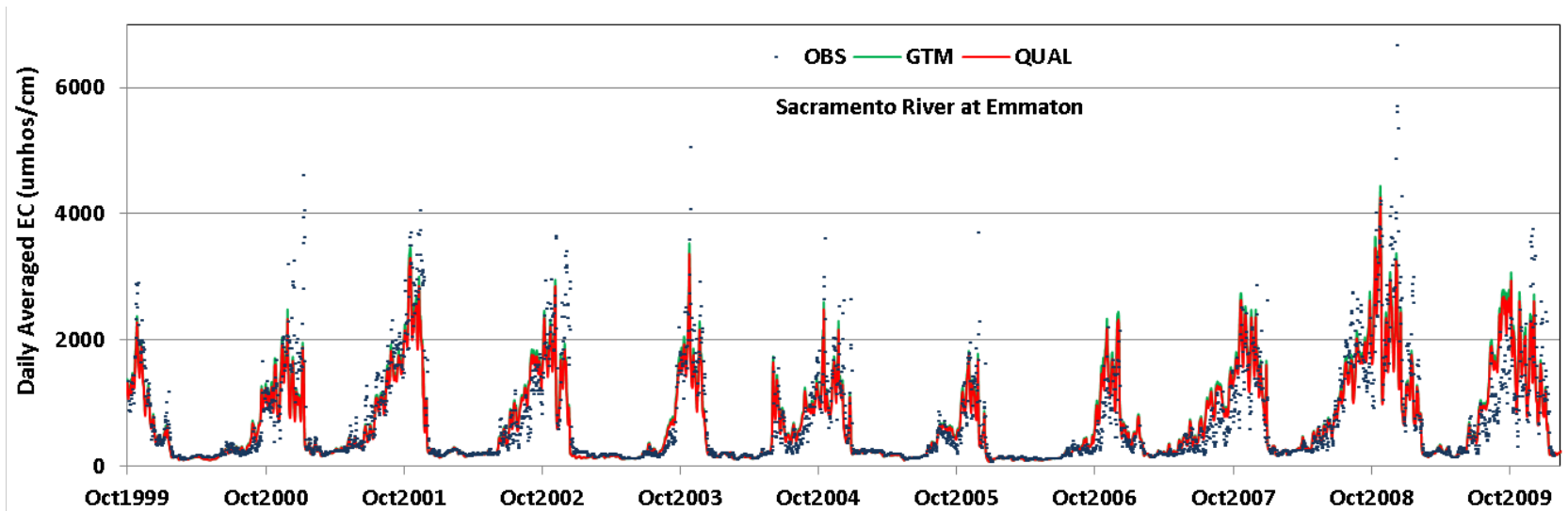
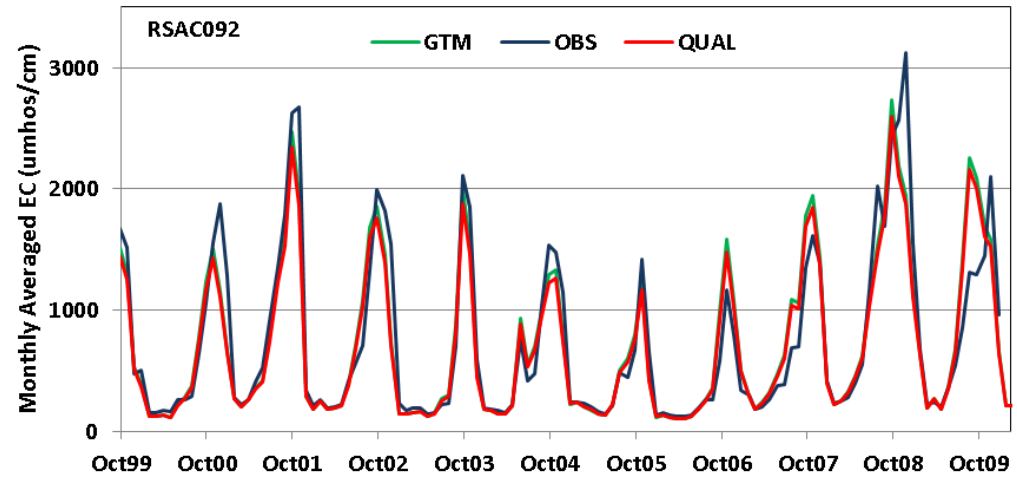
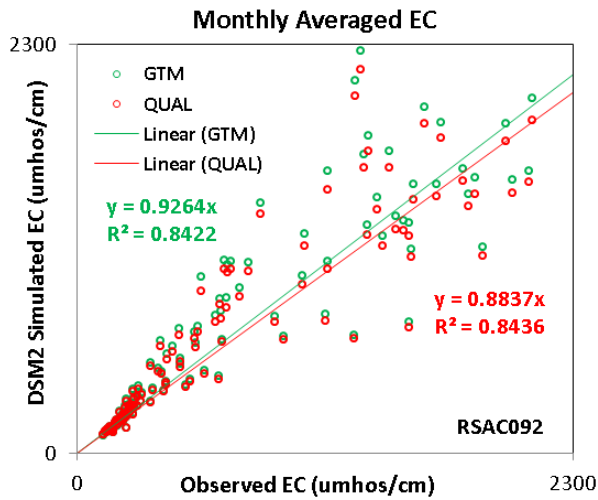


Figure 4-15 EC Results Comparison among DSM2-GTM, DSM2-QUAL, and Observed Data at Sacramento River at Emmaton

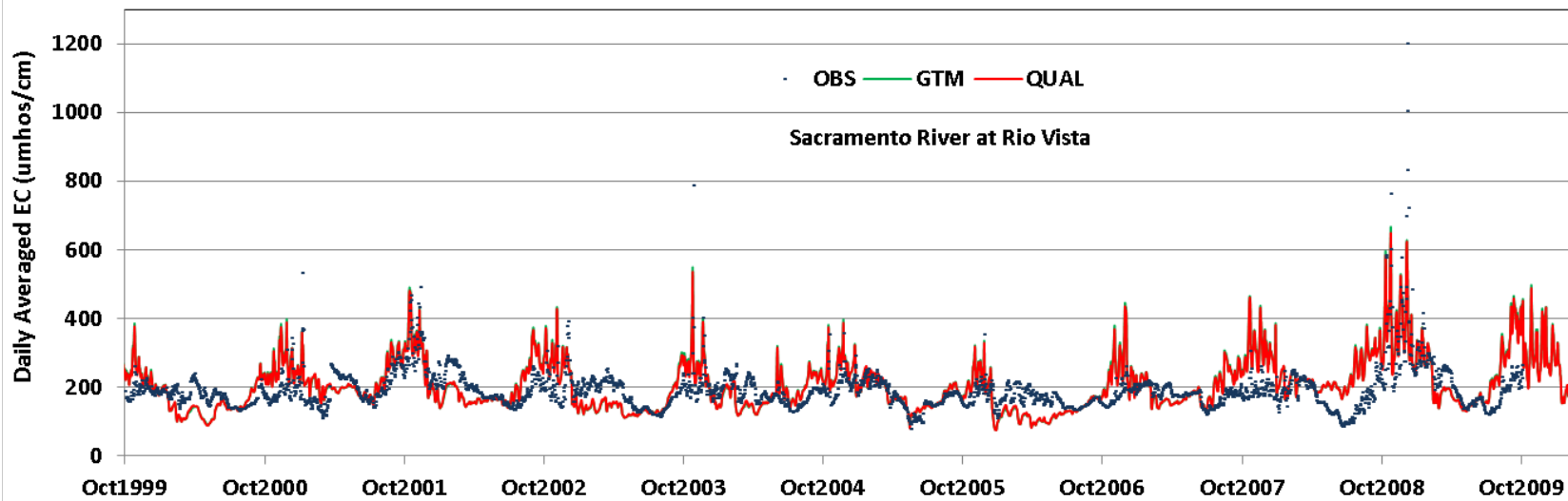
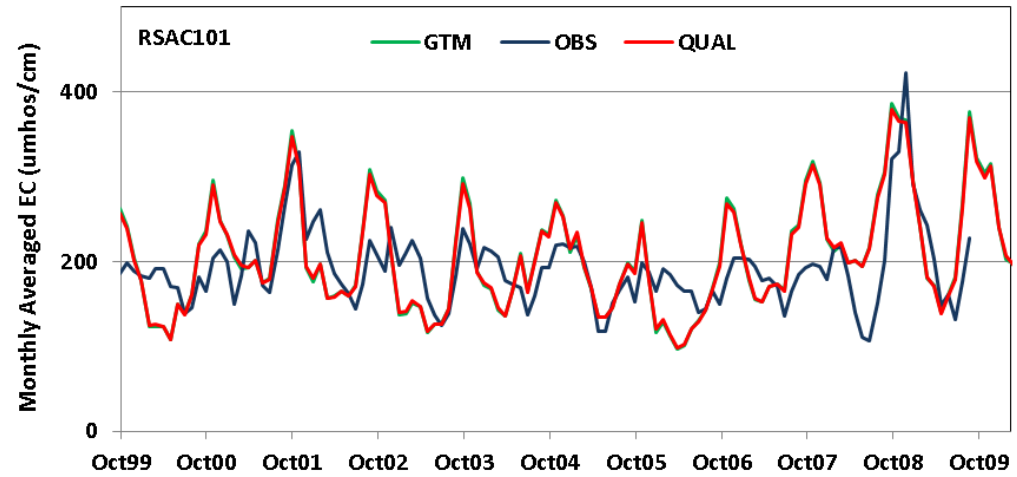
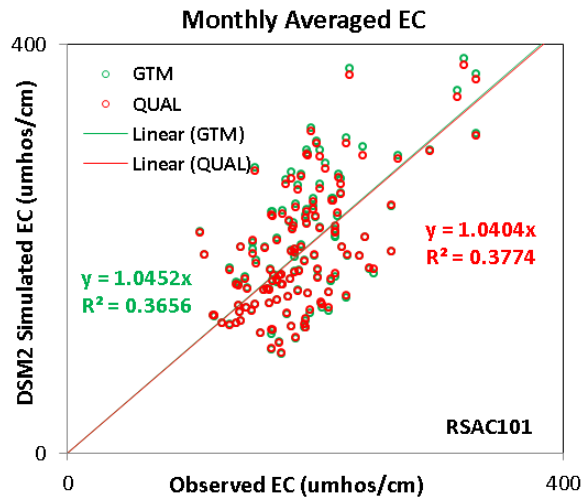


Figure 4-16 EC Results Comparison among DSM2-GTM, DSM2-QUAL, and Observed Data at Sacramento River at Rio Vista

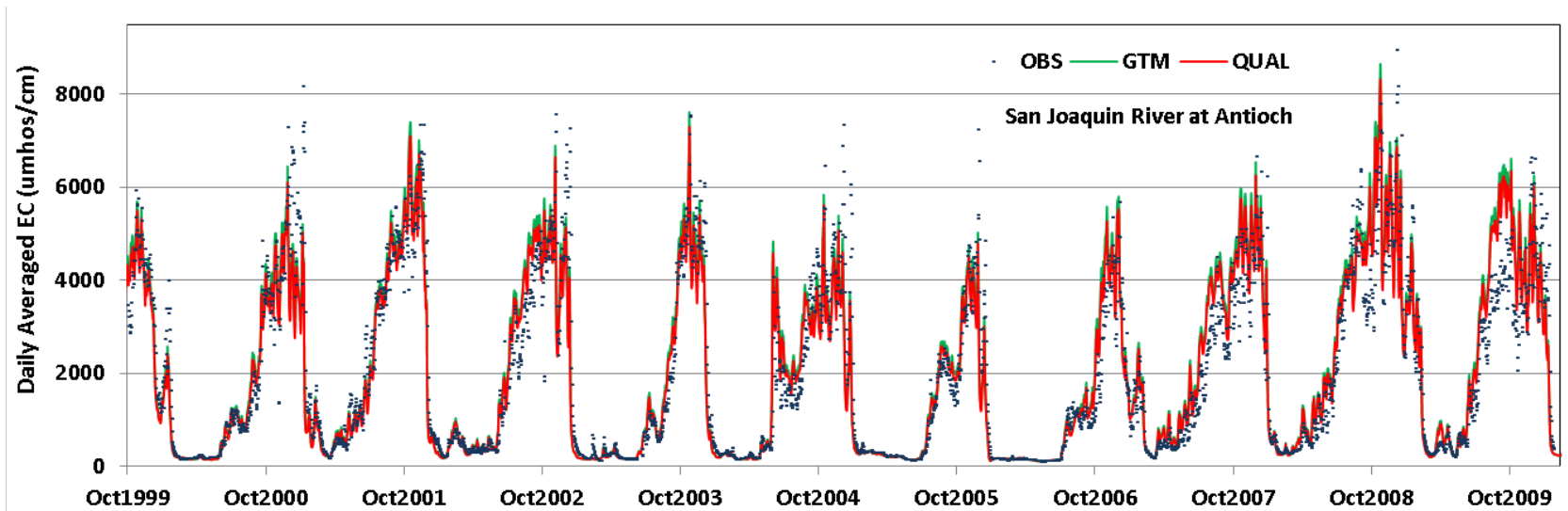
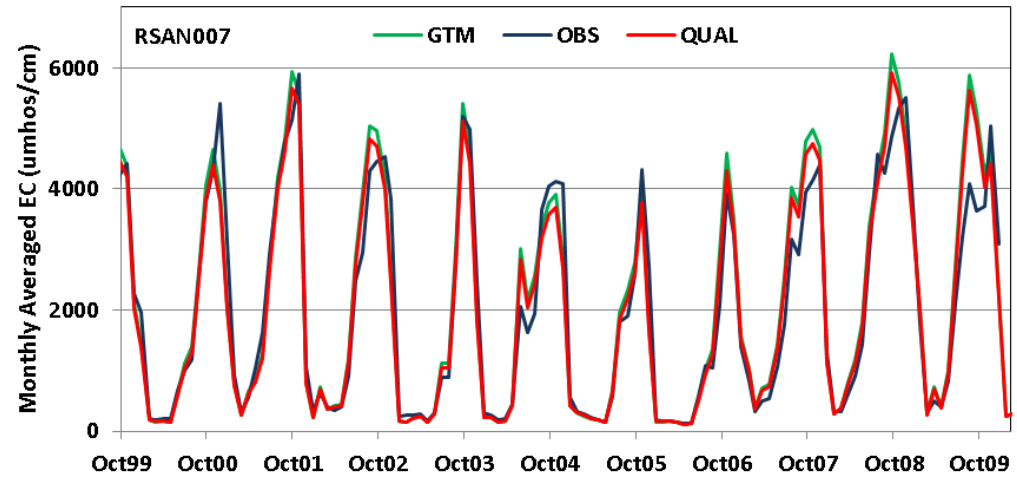
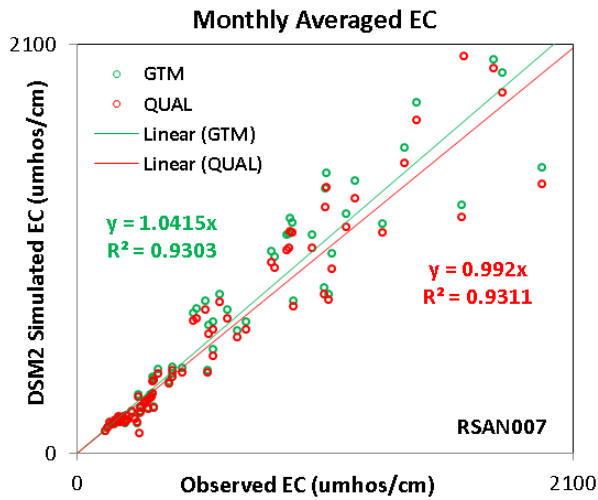


Figure 4-17 EC Results Comparison among DSM2-GTM, DSM2-QUAL, and Observed Data at San Joaquin River at Antioch

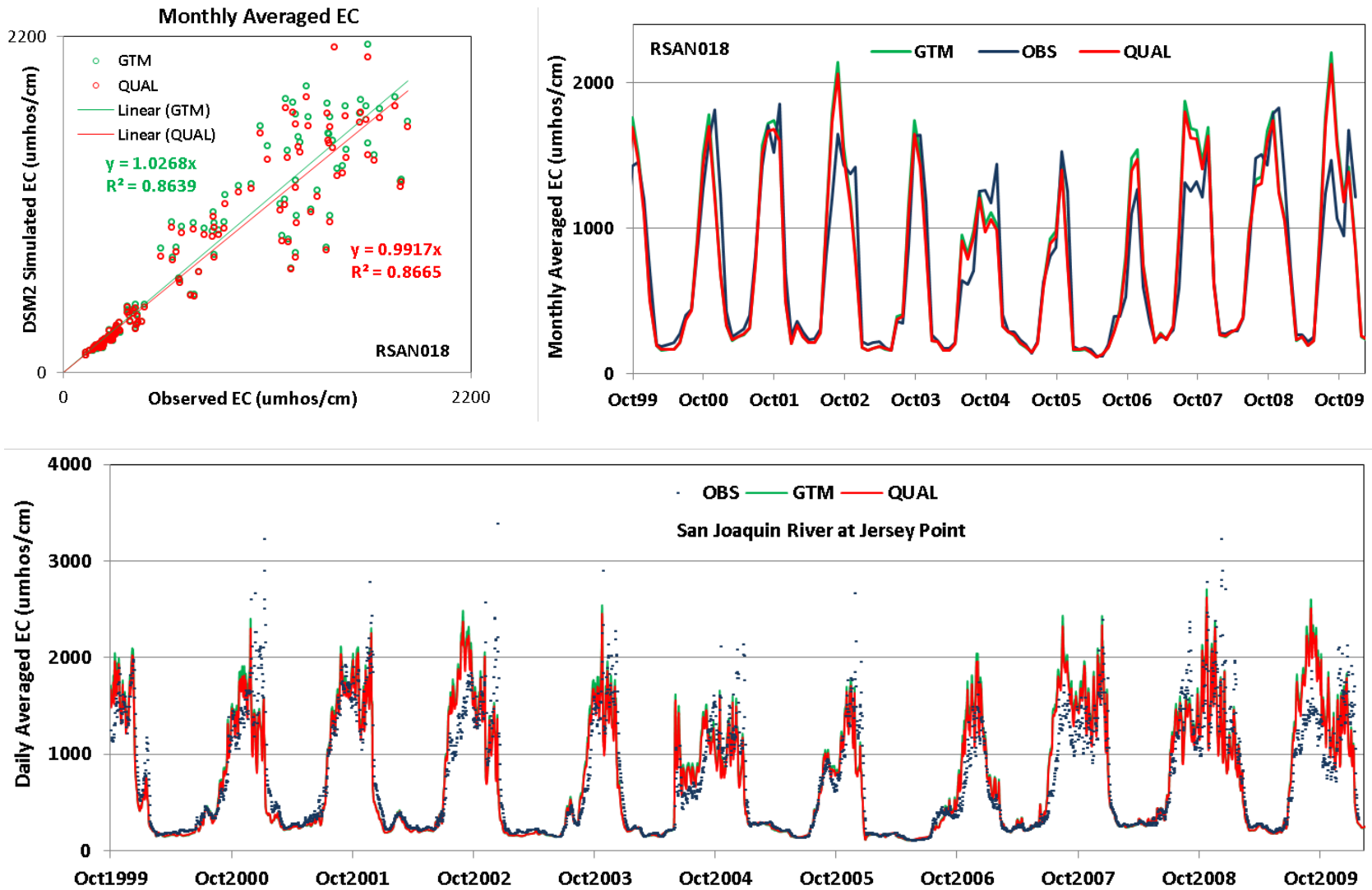


Figure 4-18 EC Results Comparison among DSM2-GTM, DSM2-QUAL, and Observed Data at San Joaquin River at Jersey Point

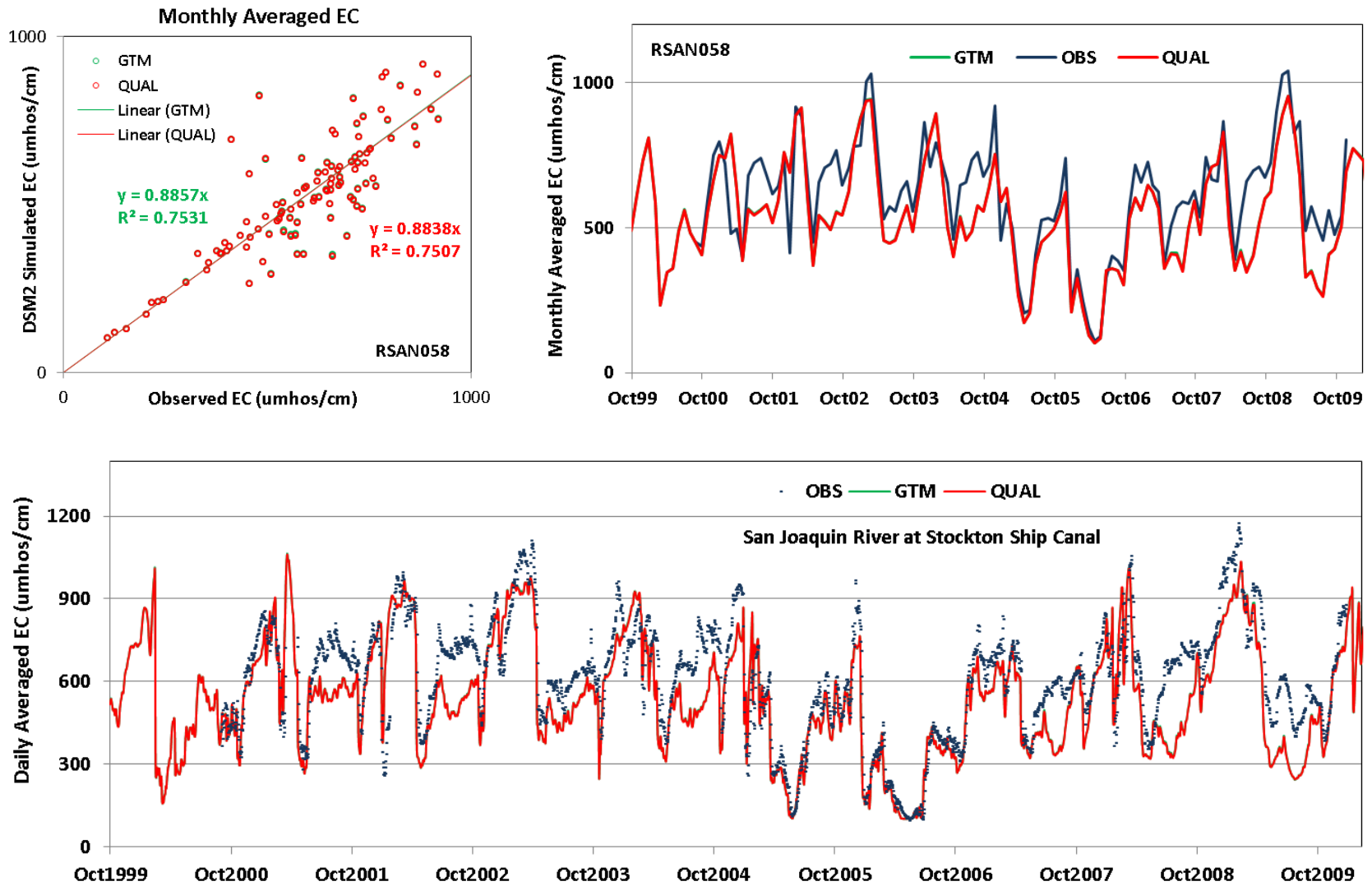


Figure 4-19 EC Results Comparison among DSM2-GTM, DSM2-QVAL, and Observed Data at San Joaquin River at Stockton Ship Canal

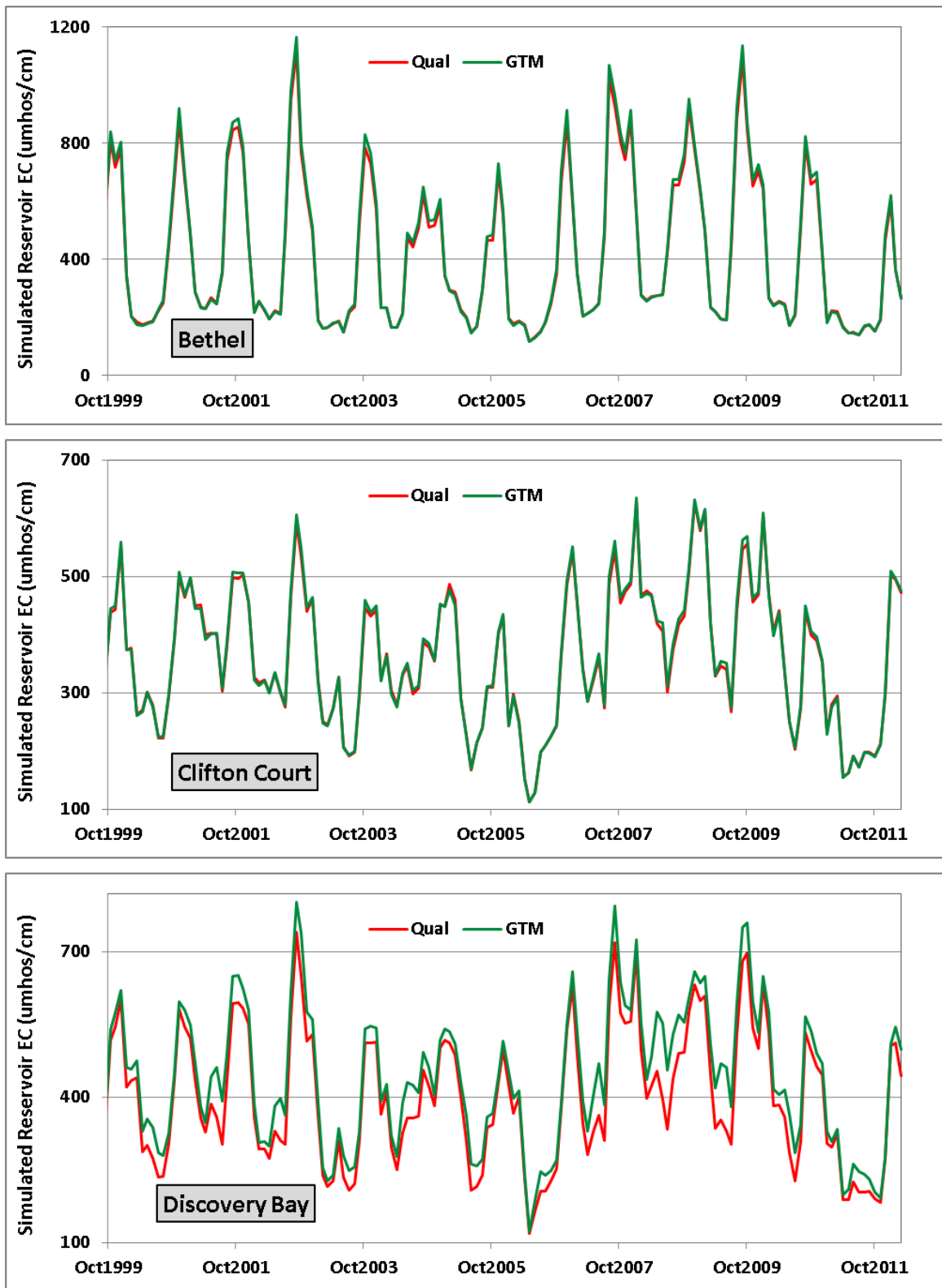


Figure 4-20 Simulated Reservoir EC Comparison (Bethel, Clifton Court, and Discovery Bay)

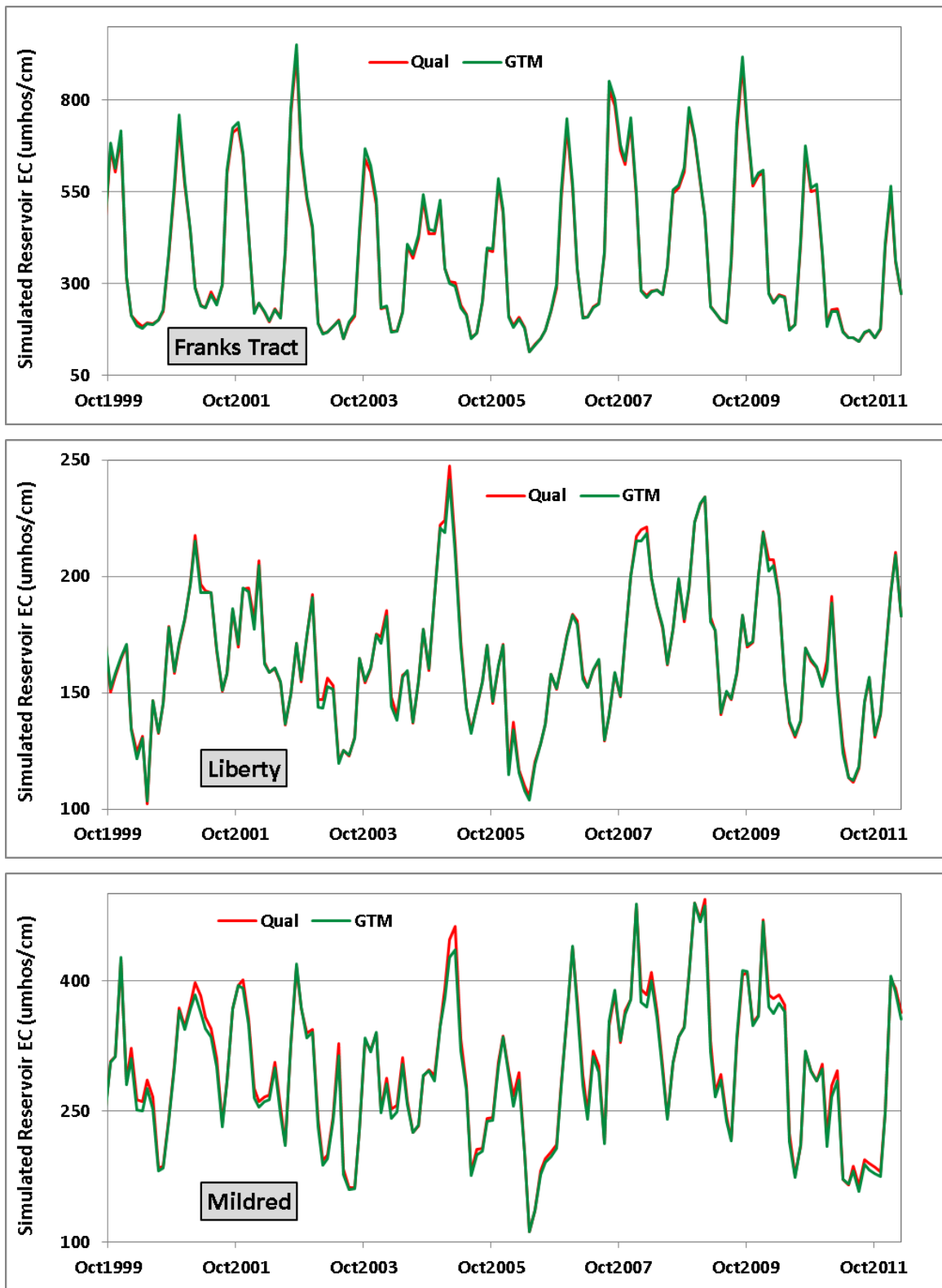


Figure 4-21 Simulated Reservoir EC Comparison (Franks Tract, Liberty, and Mildred)

4.6 Sensitivity and Stability Tests

4.6.1 Sensitivity Analysis

The goal of our sensitivity tests was to ensure that DSM2-QUAL and DSM2-GTM responded to flow perturbations the same way. We performed sensitivity tests around three areas of hydrology: 1) increasing or decreasing Sacramento River inflow by 10 percent, 2) increasing or decreasing SWP pumping by 10 percent, and 3) increasing or decreasing DICU flows by 10 percent.

Figure 4-22 shows sensitivity to changes in the Sacramento River upstream inflow at Emmaton. The monthly average is calculated from tidally filtered results. Under a decrease in Sacramento River flow, salinity is higher throughout the simulation period. Under a decrease it is lower. When Sacramento River inflow is increased, the water becomes less salty as expected. DSM2-GTM and DSM2-QUAL have similar amplitude of sensitivity as the response to the flow variation.

Figure 4-23 shows sensitivity to an increase of SWP pumping at Old River at Bacon Island. The increase in pumping raises salinity. Again, the simulated results with this flow variation, because of pumping, are still very consistent between DSM2-GTM and DSM2-QUAL. The analysis of sensitivity to an increase in DICU channel depletions also yields very similar results.

Overall, these results indicate the response from DSM2-GTM is as anticipated and is in a range that is consistent to the response of DSM2-QUAL.

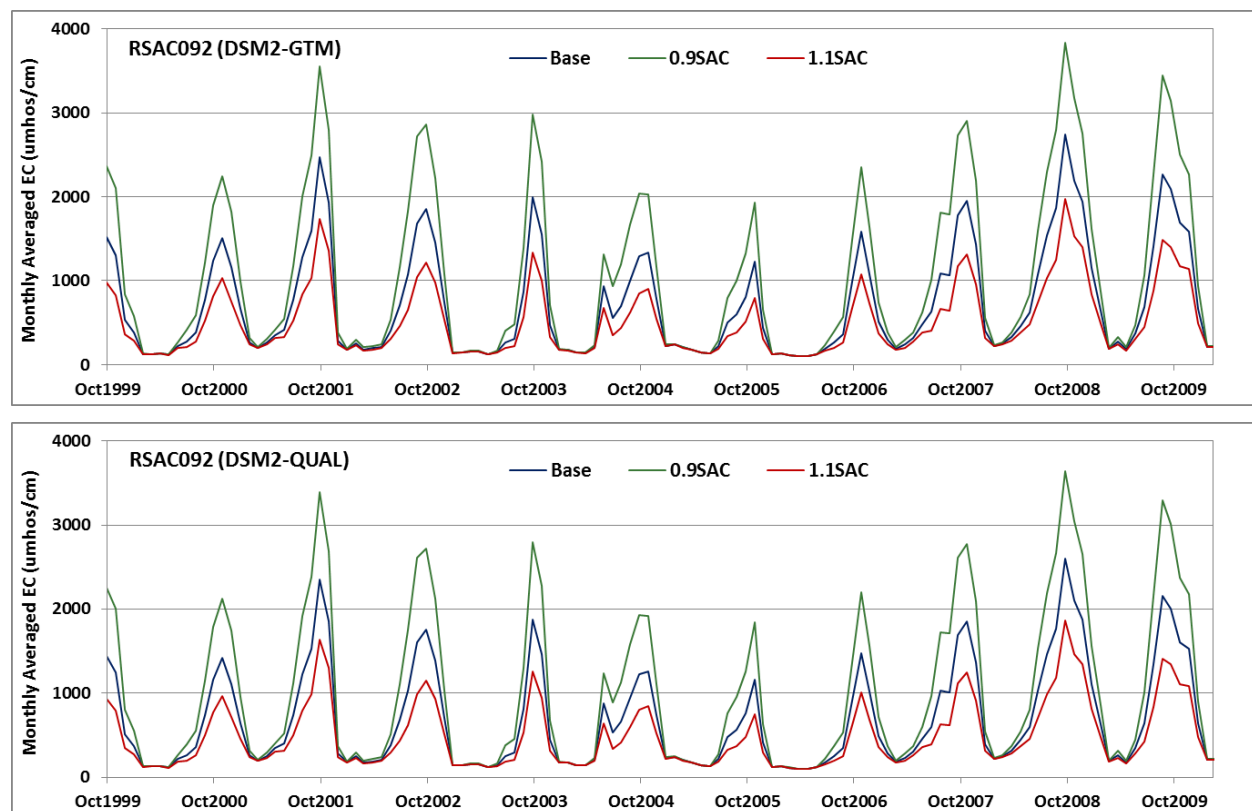


Figure 4-22 Sensitivity Analysis of Varying Sacramento Flow by 10 percent at Emmaton

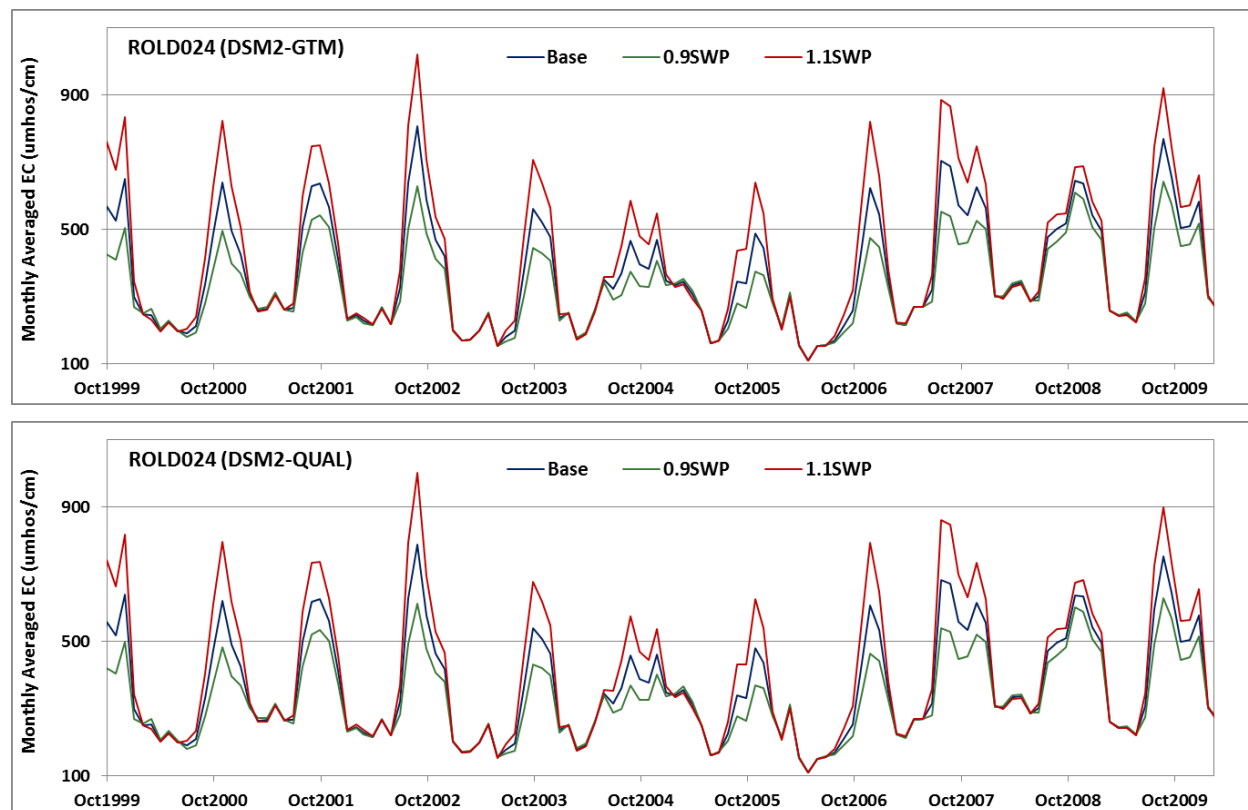


Figure 4-23 Sensitivity Analysis of Varying SWP Pumping by 10 percent at Old River at Bacon Island

4.6.2 Delta-scale Convergence Test

Any solver based on a partial differential equation should converge to the solution of that equation as the spatial and temporal step is refined. The convergence test of the Eulerian scheme on a single reach case was tested by Ateljevich et al. (2011). We verified only that this property of convergence holds over the more complex Delta network system. Note that while convergence testing is considered to be an essential test of the solver and how well it solves its target equations (verification), it is not a test against field data and a test of the success of those equations in modeling reality (validation).

For this test, the hydrodynamic information is obtained from DSM2-HYDRO with a discretization length (hydro_dx) of 5,000 ft and hydro time step of 15 minutes. The spatial step (gtm_dx) for transport in our base study is 1,000 ft. The time step is 5.0 minutes, though subcycling reduces this adaptively.

The purpose of this testing is to examine convergence and stability of this scheme on a network system. The simulation result of $dx = 250$ ft is used as the benchmark solution. The convergence test is done by assessing change in error under successive refinement of the grid each time by a factor of two. DSM2-GTM internally recalculates the time step based on the CFL number, so that as the spatial step (dx) is coarsened or refined. The time step (dt) will be coarsened or refined approximately in lockstep. The three levels of discretization used to assess convergence are $dx = 500$ ft, 1,000 ft, and 2,000 ft. The raw data set are 15-minute-instantaneous values that operated for 13 years.

Error norms relative to the benchmark are used as the measure to quantitate the difference, denoted as e . The analysis is done at individual location and evaluated separately. Three norms are used: L_1 , L_2 , and L_{inf} . L_1 norm in Eq. (21) is the absolute difference between two vectors. In a more general case of error measurement, it is scaled by the size of the vector, which is known as Mean Absolute Error (MAS). The L_2

norm in Eq. (22) is the Mean Square Error (MSE). L_{inf} norm in Eq. (23) is the maximum magnitude of the error vector.

$$L_1 = \frac{1}{N} \sum_n |e_n| \tag{21}$$

$$L_2 = \frac{1}{N} \sqrt{\sum_n e_n^2} \tag{22}$$

$$L_{inf} = \max(|e_n|) \tag{23}$$

L_1 , L_2 , and L_{inf} are calculated for three sets and data ($dx = 500$ ft, $1,000$ ft and $2,000$ ft) at each individual site. The order of convergence (P) and the ratio of the norms for those key locations are summarized in Table 4-1. To visualize the convergence as the grid goes from coarse to fine, the error norms of L_1 and L_2 against grid sizes are plotted on logarithmic scale in Figure 4-24. By looking at the values of L_1 , L_2 , and L_{inf} norms in Table 4-1, it is obvious that the error is reduced exponentially. The factor of reduction from $dx = 2,000$ ft to $dx = 1,000$ ft is much more significant than that from $dx = 1,000$ ft to $dx = 500$ ft. The ratios of the norm differences mostly are greater than 2.0 and the order of convergence is mostly between 1.0 and 2.0 for spatial steps we would consider using for most studies.

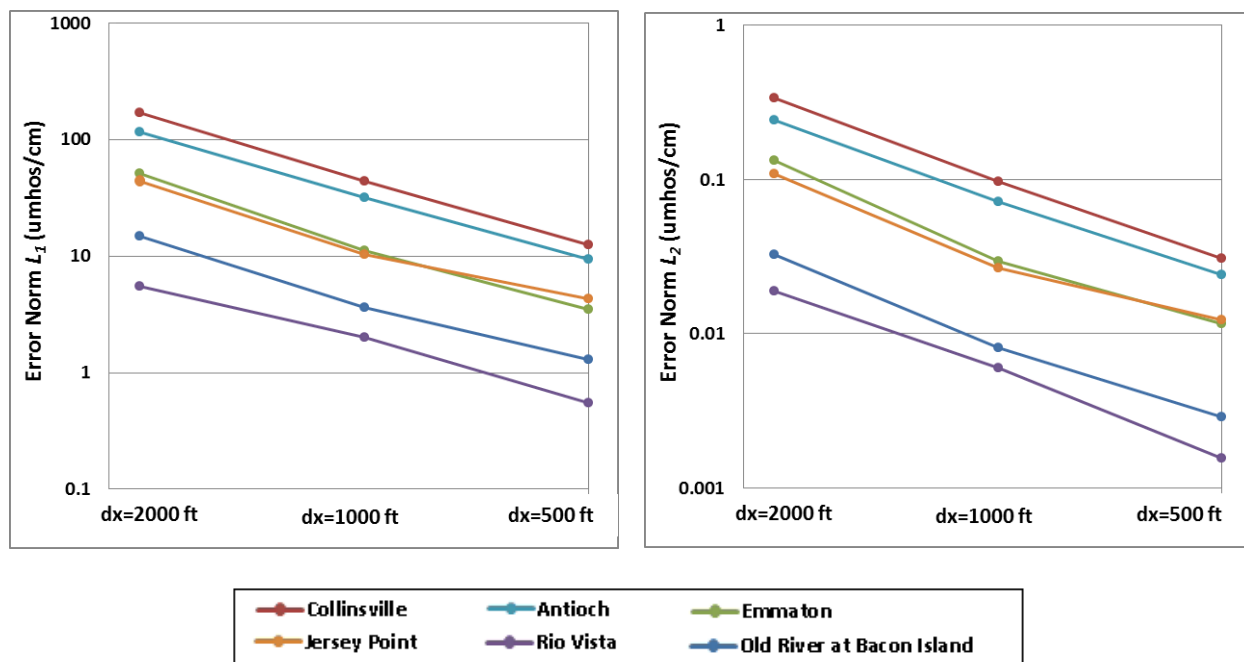


Figure 4-24 L_1 and L_2 Error Norms on Logarithmic Scale Plots

The results for gtm_dx less than $1,000$ ft are almost identical on a typical DSM2 flow field of $5,000$ ft. $Gtm_dx = 2,000$ ft is too coarse for the Delta network, whereas $gtm_dx = 1,000$ ft seems to be a good spatial step for general purpose Delta simulations. Smaller grid sizes cost more in calculation time and should be avoided unless these are needed for particular studies with sharper fronts. The differences from $gtm_dx = 500$ ft to $gtm_dx = 250$ ft are fairly small, mostly less than 10 umhos/cm in Delta locations, and that is far less than 1 percent of tidal amplitude. This is about where the point convergence falls off. DSM2-QUAL, Version 8.1 and subsequent versions show qualitative convergence

with respect to time step and parcel size with the corrections to advection and dispersion formulation (Liu et al. 2011).

Table 4-1 Results for Convergence Test

	Grid size	L_1 ($\mu\text{mho/cm}$)	L_2 ($\mu\text{mho/cm}$)	L_{inf} ($\mu\text{mho/cm}$)	Ratio		
					L_1	L_2	L_{inf}
Old River at Bacon Island	500 ft	1.2944	0.0029	8.5038	-	-	-
	1,000 ft	3.5950	0.0081	25.2857	2.7773	2.8072	2.9734
	2,000 ft	14.8277	0.0324	68.3060	4.1245	3.9829	2.7014
	P	1.3872	1.3409	0.9119	-		
Collinsville	500 ft	12.5143	0.0306	106.9648	-	-	-
	1,000 ft	44.2307	0.0967	445.3335	3.5344	3.1587	4.1634
	2,000 ft	170.8205	0.3356	666.7441	3.8620	3.4707	1.4972
	P	1.0702	1.0820	0.2830	-		
Emmaton	500 ft	3.5039	0.0117	64.4849	-	-	-
	1,000 ft	11.2394	0.0295	193.4102	3.2077	2.5219	2.9993
	2,000 ft	51.4593	0.1321	476.2666	4.5785	4.4810	2.4625
	P	1.3053	1.6214	0.8204	-		
Antioch	500 ft	9.4444	0.0242	109.6953	-	-	-
	1,000 ft	32.1238	0.0718	371.1885	3.4014	2.9608	3.3838
	2,000 ft	116.7253	0.2428	630.4229	3.6336	3.3838	1.6984
	P	1.0540	1.1228	0.4345	-		
Jersey Point	500 ft	4.3004	0.0123	55.9795	-	-	-
	1,000 ft	10.2797	0.0266	170.6326	2.3904	2.1535	3.0481
	2,000 ft	44.4614	0.1084	419.1099	4.3252	4.0811	2.4562
	P	1.6805	1.8336	0.8063	-		

Notes: P = order of convergence, $\mu\text{mho/cm}$ = micromhos per centimeter

4.7 Summary

1. DSM2-GTM accomplishments so far include integrating GTM into DSM2, accommodating special features (boundaries, junctions, external flows, reservoirs and gates), and successfully simulating EC for the full Delta using a full cycle of DSM2-HYDRO and DSM2-GTM.
2. With the historical Delta EC simulation, January 1999—April 2012, and the calibrated dispersion coefficients from current DSM2-QUAL Version 8.1, DSM2-GTM shows consistent results compared with DSM2-QUAL. DSM2-GTM also matches historical EC data at key locations fairly well. Except for some discrepancies in the South Delta area, most locations are almost identical.
3. For advection only, the numerical diffusion of the new Eulerian scheme is minimal and has been confirmed at field scale. Results of the test case are close to the results from DSM2-QUAL.

4. The Eulerian scheme has been well-tested on a single channel problem with different scenarios by Ateljevich et al. (2011). We have also done field-scale tests with reasonable convergence results.
5. Sensitivity tests indicate the response from DSM2-GTM to hydrology is as anticipated and in a range that is consistent to the response of DSM2-QUAL.
6. DSM2-GTM is stable in convergence and during years of simulation. The performance is reasonable considering it has more precise grids and tracks of the grid at each time step. Currently, it takes DSM2-GTM about 30 minutes for a 10-year simulation while it takes DSM2-QUAL 15 minutes for the same period. There may be room to improve the performance, but both are fairly fast, so this is not considered as a critical issue early in development.
7. The fixed DSM2-GTM grid offers convenience and extensibility. Sediment, dissolved oxygen, and mercury modules will be released soon.
8. A fixed grid should make visualization tools easy to implement, which has been a difficulty with DSM2-QUAL for a long time.
9. Currently, DSM2-GTM only operates off-line of DSM2-HYDRO. There is interest to conduct salinity simulation in-line with DSM2-HYDRO, partially to incorporate density-induced setup in the model and partly to allow operation of hydraulic structures based on salinity.

4.8 Acknowledgements

We want to acknowledge Fabian Bombardelli and Kaveh Zamani from University of California, Davis, for their roles in the initial development of the Eulerian solver and testing system. We thank Lianwu Liu, Ralph Finch, and Hari Rajbhandari for their helpful descriptions of DSM2-HYDRO and DSM2-QUAL aspects. We thank Jamie Anderson for initiating the sediment transport study and the collaborative effort. We also thank Branch Chief Francis Chung, Section Chief Tara Smith, and Carol DiGiorgio for their support of this project.

4.9 References

Ateljevich E, Anderson J, Zamani K, and Bombardelli FA. 2011. "Using Software Quality and Algorithm Testing to Verify a One-dimensional Transport Model." In: *Methodology for Flow and Salinity Estimates in the Sacramento-San Joaquin Delta and Suisun Marsh*. 32nd Annual Progress Report to the State Water Resources Control Board. Sacramento (CA): Bay-Delta Office. Delta Modeling Section. California Department of Water Resources.

California Department of Water Resources. 1998a. "DSM2 QUAL." In: *Methodology for Flow and Salinity Estimates in the Sacramento-San Joaquin Delta and Suisun Marsh*. 19th Annual Progress Report to the State Water Resources Control Board. Chapter 3. Sacramento (CA): Bay-Delta Office. Delta Modeling Section. California Department of Water Resources.

———. 1998b. "DSM2 Input and Output." In: *Methodology for Flow and Salinity Estimates in the Sacramento-San Joaquin Delta and Suisun Marsh*. 19th Annual Progress Report to the State Water Resources Control Board. Chapter 5. Sacramento (CA): Bay-Delta Office. Delta Modeling Section. California Department of Water Resources.

Berger M, Aftosmis MJ, and Murman SM. 2005. "Analysis of Slope Limiters on Irregular Grids." 43rd AIAA Aerospace Sciences Meeting. January 10–13, 2005. Reno, NV. NAS Technical Report NAS-05-007. American Institute of Aeronautics and Astronautics Paper 2005-0490.

Browns LC and Barnwell TO. 1987. *The Enhanced Stream Water Quality Models QUAL2E and QUAL2E-UNCAS: Documentation and Users Manual*. U.S. Environmental Protection Agency. Athens (GA): EPA 600/3-87/007.

Colella P and Puckett EG. 1998. Modern Numerical Methods for Fluid Flow. Class note at the University of California, Davis.

Fischer HB, List ET, Imberger J, and Brooks NH. 1979. *Mixing in Inland and Coastal Waters*. New York (NY): Academic Press.

Hsu E, Ateljevich E, Sandhu P. 2014. "DSM2-GTM." In: *Methodology for Flow and Salinity Estimates in the Sacramento-San Joaquin Delta and Suisun Marsh*. 35th Annual Progress Report to the State Water Resources Control Board. Sacramento (CA): Bay-Delta Office. Delta Modeling Section. California Department of Water Resources.

Jobson HE. 1997. *Enhancements to the branched Lagrangian Transport Modeling System*. Reston (VA): U.S. Geological Survey. Water Resources Investigations Report 97-4050.

Jobson HE and Schoellhamer DH. 1987. *Users Manual for a Branched Lagrangian Transport Model*. U.S. Geological Survey, Water Resources Investigation Report 87-4163.

Leveque RJ. 2002. *Finite Volume Methods for Hyperbolic Problems*. Cambridge (UK): Cambridge University Press.

Liu L, Ateljevich E, Sandhu P. 2013. "DSM2 Version 8.1 Calibration with NAVD88 Datum." In: *Methodology for Flow and Salinity Estimates in the Sacramento-San Joaquin Delta and Suisun Marsh*. 34th Annual Progress Report to the State Water Resources Control Board. Sacramento (CA): Bay-Delta Office. Delta Modeling Section. California Department of Water Resources.

———. 2012. "Improved Geometry Interpolation in DSM2-Hydro." In: *Methodology for Flow and Salinity Estimates in the Sacramento-San Joaquin Delta and Suisun Marsh*. 33rd Annual Progress Report to the State Water Resources Control Board. Sacramento (CA): Bay-Delta Office. Delta Modeling Section. California Department of Water Resources.

Liu L and Ateljevich E. 2011. "Improvement to the DSM2-QUAL: Part 1." In: *Methodology for Flow and Salinity Estimates in the Sacramento-San Joaquin Delta and Suisun Marsh*. 32nd Annual Progress Report to the State Water Resources Control Board. Sacramento (CA): Bay-Delta Office. Delta Modeling Section. California Department of Water Resources.

Natarajan EP. 2005. KLU - a high performance sparse linear system solver for circuit simulation problems. Master's Thesis. Gainesville (FL): Computer & Information Science and Engineering Department. University of Florida.

Saltzman J. 1994. "An unsplit 3D upwind method for hyperbolic conservation laws." *Journal of Computational Physics* (115): pp. 153-168.

Van Leer B. 1997. "Towards the ultimate conservative difference scheme, IV. A new approach to numerical convection". *Journal of Computational Physics* (23): pp. 276-299.

